Computational and Structural Biotechnology Journal 20 (2022) 1654–1669

COMPUTATIONAL AND STRUCTURAL BIOTECHNOLOGY JOURNAL

journal homepage: www.elsevier.com/locate/csbj

Dissecting chicken germ cell dynamics by combining a germ cell tracing transgenic chicken model with single-cell RNA sequencing

Deivendran Rengaraj [a,1], Dong Gon Cha [b,1], Hong Jo Lee [a,1], Kyung Youn Lee [a], Yoon Ha Choi [c,b], Kyung Min Jung [a], Young Min Kim [a], Hee Jung Choi [a], Hyeon Jeong Choi [a], Eunhui Yoo [a], Seung Je Woo [a], Jin Se Park [a], Kyung Je Park [a], Jong Kyoung Kim [c,b,*], Jae Yong Han [a,*]

[a] Department of Agricultural Biotechnology, and Research Institute of Agriculture and Life Sciences, Seoul National University, Seoul 08826, South Korea
[b] Department of New Biology, DGIST, Daegu 42988, South Korea
[c] Department of Life Sciences, Pohang University of Science and Technology (POSTECH), Pohang 37673, South Korea

ARTICLE INFO

Article history:
Received 17 December 2021
Received in revised form 30 March 2022
Accepted 31 March 2022
Available online 2 April 2022

Keywords:
Transgenic chicken
DAZL gene
Genome editing
Germ cell
Single-cell RNA sequencing

ABSTRACT

Avian germ cells can be distinguished by certain characteristics during development. On the basis of these characteristics, germ cells can be used for germline transmission. However, the dynamic transcriptional landscape of avian germ cells during development is unknown. Here, we used a novel germ-cell-tracing method to monitor and isolate chicken germ cells at different stages of development. We targeted the deleted in azoospermia like (*DAZL*) gene, a germ-cell-specific marker, to integrate a green fluorescent protein (*GFP*) reporter gene without affecting endogenous *DAZL* expression. The resulting transgenic chickens (*DAZL::GFP*) were used to uncover the dynamic transcriptional landscape of avian germ cells. Single-cell RNA sequencing of 4,752 male and 13,028 female *DAZL::GFP* germ cells isolated from embryonic day E2.5 to 1 week post-hatch identified sex-specific developmental stages (4 stages in male and 5 stages in female) and trajectories (apoptosis and meiosis paths in female) of chicken germ cells. The male and female trajectories were characterized by a gradual acquisition of stage-specific transcription factor activities. We also identified evolutionary conserved and species-specific gene expression programs during both chicken and human germ-cell development. Collectively, these novel analyses provide mechanistic insights into chicken germ-cell development.

1. Introduction

Germ cells produce types of cells that transmit genetic information to the next generation. Compared with germ cells of other animal species, avian germ cells have unique developmental characteristics in terms of specification, migration, and development [1]. Two modes of germ cells specification were reported in the vertebrate species: epigenesis mode in mammals; and preformation mode in several lower vertebrate species [2]. In particularly, avian germ cells are known to be specified by preformation mode, in which maternally inherited components called "germ plasm" play critical role in the specification of germ cells and maintaining the integrity of germ cells. The germ plasm consists of energy-rich mitochondria, and a set of RNAs and proteins, including the germ-cell-specific markers DEAD-box helicase (*DDX4*) and deleted in azoospermia like (*DAZL*) [3,4]. The precursors of chicken germ cells, called primordial germ cells (PGCs), are detected as early as Eyal-Giladi and Kochav (EGK) [5] stage-III of embryogenesis on the basis of expression of the *DAZL* [4]. Germ cells scattered in the central region of EGK stage-X embryos are incorporated into the germinal crescent region of Hamburger and Hamilton (HH) [6] stage-4 embryos. These germ cells then circulate through the blood to colonize bilateral-embryonic gonads at around HH stage 24. After colonization, germ cells actively proliferate and differentiate in a sexually dimorphic manner [7].

During embryogenesis in several species, common germ-cell developmental events include migration, embryonic gonad settlement, and sex-specific differentiation. Distinct molecular networks regulate these events in both male and female germ cells [8,9]. Avian germ cells also dynamically proliferate and differentiate:

* Corresponding authors at: POSTECH, 77 Cheongam-ro, Nam-gu, Pohang-si, Gyeongsangbuk-do 37673, South Korea (J.K. Kim). Seoul National University, 1 Gwanak-ro, Gwanak-gu, Seoul 08826, South Korea (J.Y. Han).
E-mail addresses: blkimjk@postech.ac.kr (J.K. Kim), jaehan@snu.ac.kr (J.Y. Han).
[1] These authors contributed equally to this work.

https://doi.org/10.1016/j.csbj.2022.03.040
2001-0370/

male germ cells enter mitotic arrest, and female germ cells enter meiotic arrest [7,10–12]. However, studies of germ-cell dynamics during embryogenesis are limited because surface markers to isolate germ cells at each developmental stage are not available.

We combined a novel germ-cell-tracing method with time-resolved single-cell RNA sequencing (scRNA-seq) to explore chicken germ-cell dynamics at single-cell resolution. We used the clustered regularly interspaced short palindromic repeats (CRISPR) and CRISPR-associated protein 9 (CRISPR/Cas9) gene-editing system to insert a green fluorescent protein (*GFP*)-expression cassette into *DAZL* through nonhomologous end joining (NHEJ) to produce *DAZL::GFP* transgenic chickens. DAZL, an RNA-binding protein and DAZ-family member, is a master factor critical for germ-cell development and maintenance in diverse vertebrate and invertebrate species. DAZL binds and regulates thousands of mRNAs 3′ untranslated regions (3′ UTRs) during different stages of germ-cell development [13]. In chickens, DAZL mRNA and protein are components of germ plasm, in which the zygote inherits to specify germ cells [4]. DAZL mRNA and protein are also continuously expressed at various stages of chicken germ-cell development (including specification, migration, differentiation, and gametogenesis) [4,14]. Our main objectives of this study are to produce *DAZL::GFP* transgenic chickens without affecting endogenous DAZL expression, to isolate pure population of male and female germ cells from the *DAZL::GFP* transgenic chickens at embryonic day 2.5 (E2.5) to 1 week post-hatch, and to analyze the isolated cells by using scRNA-seq for investigating the transcriptional landscape, cellular heterogeneity and developmental trajectories of chicken germ cells.

2. Materials and methods

2.1. Animals

The management and experimental use of chickens were approved by the Institute of Laboratory Animal Resources, Seoul National University (SNU-190401-1-1). The experimental animals were cared according to a standard management program at the University Animal Farm, Seoul National University, Korea. The procedures for animal management, reproduction, and embryo manipulation adhered to the standard operating protocols of Animal Genetic Engineering Laboratory, Seoul National University.

2.2. Construction of CRISPR/Cas9 and donor plasmids

All-in-one CRISPR/Cas9 plasmids targeting the last intron of chicken *DAZL* were constructed by using the multiplex-CRISPR/Cas9 plasmid-construction kit (provided by Takashi Yamamoto) (Addgene Kit #1000000054) [15]. A neomycin-resistance gene (regulated by the thymidine-kinase promoter) was ligated into the *Not*I (New England Biolabs, Ipswich, MA, USA) sites of the CRISPR/Cas9 plasmids. To insert *DAZL*-targeting gRNA sequences into the CRISPR/Cas9 plasmids, sense and antisense oligonucleotides were designed (Table S1) and synthesized (Bionics, Seoul, Korea). The oligonucleotides were denatured and reannealed with the following thermocycling conditions: 30 sec at 95 °C, 2 min at 72 °C, 2 min at 37 °C, and 2 min at 25 °C. To tag chicken *DAZL*, a donor plasmid was synthesized to contain the last intron and exon of *DAZL* (including the gRNA-recognition sequence) in frame with a T2A peptide and GFP expression cassette (Bioneer, Daejeon, Korea). The neomycin-resistance gene with a thymidine-kinase promoter was inserted into the 3′-downstream region of the synthesized plasmid.

2.3. Cell culture

White Leghorn (WL) PGCs retrieved from male gonads at E6 by magnetic-activated cell-sorting (MACS) method [16] were maintained and sub-passaged on knockout Dulbecco's minimum essential medium (DMEM; Invitrogen, Carlsbad, CA, USA) supplemented with 20% fetal bovine serum (FBS; Invitrogen); 2% chicken serum (Sigma-Aldrich, St. Louis, MO, USA); 1× nucleosides (Millipore, Temecula, CA, USA); 2 mM L-glutamine; 1× nonessential amino acids; 0.2% β-mercaptoethanol; 10 mM sodium pyruvate; 1× antibiotic–antimycotic (Invitrogen); and 10 ng/mL human basic fibroblast growth factor (Sigma-Aldrich). Chicken PGCs were cultured in an incubator at 37 °C under an atmosphere of 5% CO_2 and 60–70% relative humidity. The PGCs were sub-cultured onto mitomycin-inactivated mouse embryonic fibroblasts at five-day or six-day intervals via gentle pipetting.

2.4. Transfection and G418 selection of PGCs for targeted gene insertion

To edit chicken PGC genomes, 1×10^5 PGCs were co-transfected with donor plasmids (2 μg) and CRISPR/Cas9 plasmids (2 μg) using 4 μL Lipofectamine 2000 reagent (Thermo Fisher–Invitrogen, Carlsbad, CA, USA) suspended in 1 mL Opti-MEM (Thermo Fisher–Invitrogen). After 4 h, the transfection mixture was replaced with PGC culture medium. Geneticin Selective Antibiotic (300 μg/mL) (G418; GIBCO Invitrogen, Grand Island, NY, USA) was added to the culture medium 1 day after transfection. G418 selection was performed for up to 3 weeks. After G418 selection, genomic DNA was extracted from PGCs. Regions encompassing the CRISPR/Cas9-targeted sites were amplified by using specific primer sets (Table S1). For sequencing analysis, the amplicons were cloned into the pGEM-T-easy vector (Promega, Madison, WI, USA) and sequenced by using an ABI Prism 3730 XL DNA Analyzer (Thermo Fisher-Applied Biosystems, Foster City, CA, USA). Sequences were compared with assembled genome sequences by using BLAST (https://blast.ncbi.nlm.nih.gov).

2.5. Production of DAZL::GFP transgenic chickens

To produce a *DAZL::GFP* transgenic chicken, a window was cut into the sharp end of a Korean-Ogye (*i*/*i*)-recipient egg, and over 3,000 *DAZL::GFP* WL PGCs (*I*/*I*) were transplanted into the dorsal aorta of the HH stage 14–17 recipient embryo. The egg window was sealed with parafilm, and the egg was incubated with the sharp end down until hatching. After sexual maturation, sperm from male recipient chickens (*I* or *i*) were evaluated by breed-specific PCR, and the chickens with WL sperm (*I*) were mated with WT females (*i*/*i*). Germline-chimeric chickens were identified by offspring feather color (*I*/*i*) and the individual donor PGC-derived chickens (*I*/*i*) were further validated by subsequent genomic DNA analysis to identify targeted gene insertion.

2.6. Detection of targeted gene insertion and off-target effects

To identify modified alleles in the *DAZL::GFP* PGCs and in transgenic chickens, genomic DNA was analyzed by using knock-in PCR. All reactions were performed under the same conditions: a 20-μL volume containing genomic DNA (100 ng); 1× PCR buffer; 10 mM each dNTP; 10 pmol each amplification primers (Table S1); and 0.5 U *Taq* polymerase (Bionics). The following thermocycling conditions were used: 2 min at 95 °C; 35 cycles of 20 sec at 95 °C, 40 sec at 60 °C, and 30 sec at 72 °C; and 5 min at 72 °C. For sequencing, amplicons were ligated into pGEM-T-easy vector and sequenced as described.

To identify off-target effects, putative off-target sites were predicted for the *DAZL::GFP* transgenic chickens by using web-based CRISPR off-target prediction software (https://crispr.mit.edu/). Each site was validated manually by using TA cloning. Clones were sequenced as described.

2.7. Reverse-transcription PCR and quantitative reverse-transcription PCR analysis

Total RNA was isolated from *DAZL::GFP* PGCs and WT cultured PGCs by using TRIzol reagent (Thermo Fisher Scientific). For reverse-transcription PCR (RT-PCR) and quantitative reverse-transcription PCR (qRT-PCR), total RNA (1 μg) was used as a template for cDNA synthesis with the SuperScript III First-Strand Synthesis System (Thermo Fisher Scientific). The cDNA was serially diluted (5-fold) and quantitatively equalized for PCR amplification. For each target, the same amplification primers were used for both RT-PCR and qRT-PCR (Table S1). RT-PCR was performed in a 20-μL volume containing 2 μL cDNA; 1× PCR buffer; 10 mM each dNTPs; 10 pmol each amplification primers; and 0.5 U *Taq* polymerase (Bionics). The following thermocycling conditions were used: 2 min at 95 °C; 35 cycles of 20 sec at 95 °C, 40 sec at 60 °C, 30 sec at 72 °C; and 5 min at 72 °C. qRT-PCR was performed in a 20-μL volume containing 2 μL cDNA; 1× PCR buffer; 10 mM each dNTP; 10 pmol each amplification primers; 1× EvaGreen (Biotium, Hayward, CA); and 0.5 U *Taq* polymerase. Amplification was monitored by using the CFX96 real-time PCR detection system on a C1000 thermal cycler (Bio-Rad Laboratories, Hercules, CA, USA). Thermocycling conditions for qRT-PCR were as follows: 95 °C for 3 min; and 40 cycles of 95 °C for 30 sec, 59 °C for 30 sec, and 72 °C for 30 sec. Melting-curve profiles were analyzed for all amplicons. Each sample was measured in triplicate, and relative gene expression was calculated after normalization with a housekeeping gene and control/reference sample ($2^{-\Delta\Delta Ct}$ method, where control/reference = 1).

2.8. Immunocytochemistry analysis

To validate the expression of DAZL protein, *DAZL::GFP* PGCs and WT cultured PGCs were harvested, fixed with 4% paraformaldehyde at room temperature (RT) for 10 min, and permeabilized with 0.1% Triton X-100 at RT for 10 min. After washing three times with phosphate-buffered saline (PBS), cells were blocked with a blocking buffer (PBS; 5% goat serum; 1% bovine serum albumin [BSA]) at RT for 1 h. Then, the cells were incubated at 4 °C overnight with rabbit anti-cDAZL polyclonal antibodies [4]. After washing three times with PBS, cells were incubated with secondary antibodies (anti-rabbit IgG) conjugated with Alexa Fluor 594 (Invitrogen) at RT for 1 h. Finally, cells were mounted by using Prolong Gold anti-fade reagent with 4′,6-diamidino-2-phenylindole and visualized by using a fluorescence microscope (Ti-U, Nikon, Tokyo, Japan).

2.9. Whole-mount and immunohistochemistry analysis

DAZL::GFP chicken embryos at different embryonic stages (HH stage 4 [18–19 h of development], HH stage 27 [E6], and HH stage 35 [E9]) were collected. Then, GFP expression in whole embryos (at HH stage 4), gonads with mesonephros (at E6), and whole gonads (at E9) was examined by using a fluorescence microscope (Ti-U). Next, the left-side gonads of the male and female *DAZL::GFP* chickens at different developmental stages (E6, E8, E12, E16, hatch, and 1 week post-hatch) were collected and subjected to immunohistochemistry to detect of GFP expression in germ cells. Gonads were embedded in paraffin and sectioned (8–10 μm thickness). After deparaffinization, sections were washed three times with PBS and blocked with blocking buffer at RT for 1 h. Sections were then incubated at 4 °C overnight with rabbit anti-GFP antibodies (Invitrogen). After washing three times with PBS, the sections were incubated with secondary antibodies (anti-rabbit IgG) conjugated with Alexa Fluor 488 (Abcam, Cambridge, UK) at RT for 1 h. Finally, the sections were mounted and visualized using a confocal fluorescence microscope (Carl Zeiss, Jena, Germany).

2.10. Preparation of DAZL::GFP germ cells for scRNA-seq

DAZL::GFP germ cells at various stages of embryogenesis were collected from either blood (at E2.5) or from gonads (at E6, E8, E12, E16, hatch, and 1 week post-hatch). To sample germ cells from E2.5 embryos, circulating embryonic blood from male and female embryos was extracted separately using a microneedle and was resuspended in PBS containing 1% BSA for fluorescence-activated cell sorting (FACS). The pooled left-side gonads of the male and female *DAZL::GFP* chicken at respective time (E6, E8, E12, E16, hatch, and 1 week post-hatch) were pooled separately and treated with Hank's Balanced Salt Solution (Gibco Invitrogen) containing 0.05% trypsin–EDTA (Gibco Invitrogen) and incubated at 37 °C for 10 min. During incubation, cells were gently pipetted every 2 min. After incubation, trypsin–EDTA was inactivated by adding the same volume of DMEM containing 5% FBS. Cells were harvested by centrifugation (1,250 rpm; 5 min), and washed with PBS. Cells were resuspended in PBS containing 1% BSA and filtered through a 40-μm cell strainer (Falcon™ 352340, Fisher Scientific, Hampton, NH, USA). The sex of E2.5, E6, and E8 embryos was determined (at E2.5) by sex-discriminating PCR of blood samples [17]. The sex of embryos at E12, E16, hatch, and 1 week post-hatch was determined by gonad morphology. Finally, cells were stained with propidium iodide (PI) to isolate live cells, and GFP^+/PI^- cells were sorted by using a BD FACS Aria III (BD Biosciences, San Jose, CA, USA) for scRNA-seq. In addition, another batch of *DAZL::GFP* germ cells were isolated at the representative times, including E6, E12, E16, hatch and 1 week post-hatch, for the examination of gene expression by qRT-PCR. The methods for the isolation of total RNA, cDNA synthesis, and gene amplification are same as mentioned above.

2.11. scRNA-seq

Libraries for scRNA-seq were prepared by using the Chromium Single Cell 3′ GEM, Library & Gel Bead Kit v3 (PN-1000075, 10X Genomics, Pleasanton, CA, USA); Chromium Single Cell B Chip Kit (PN-1000073, 10X Genomics); and Chromium i7 Multiplex Kit (PN-120262, 10X Genomics). Cells were resuspended in PBS containing 0.04% BSA and diluted to ~2×10^5 to ~1×10^6 cells/mL. Cells were mixed with a reverse-transcription master mix and loaded onto B chip channels to capture of ~800 to ~5,000 single-cell transcriptomes. Gel bead-in emulsions (GEMs) were generated by using Chromium Controller (10X Genomics). Reverse transcription was conducted by using a C1000 Touch thermal cycler (Bio-Rad). DNA was purified and libraries were constructed according to the manufacturer's instructions. The qualities of amplified cDNAs and of the constructed libraries were assessed by using Bioanalyzer (Agilent Technologies, Santa Clara, CA, USA). Libraries were sequenced with a 2× 100-bp paired-end protocol on a Novaseq-6000 platform (Illumina, San Diego, CA, USA) to generate at least 40,000 read pairs per cell.

2.12. scRNA-seq data preprocessing

Raw fastq files were processed using the CellRanger pipeline, version 3.1.0. The fasta and GTF files for chicken genome (GRCg6a) were modified to include the *DAZL-GFP* insert sequence. The cDNA

sequences were mapped to the modified-chicken genome by using STAR, version 2.5.1b, aligner [18] with the GRCg6a.99 GTF file. A gene-by-cell count matrix was generated by using default parameters. To remove empty droplets while capturing single cells, the EmptyDrops function of DropletUtils, version 1.8.0, R package [19] was used (with FDR < 0.05). Low-quality cells were excluded by using different cutoff thresholds for different samples. The cutoff thresholds were determined by visually inspecting outliers in the principal component analysis (PCA) plot on the quality-control metrics using the calculateQCMetrics function of the scater, version 1.16.1, R package [20].

To remove cell-specific biases, cells were clustered by using the quickCluster function of the scran, version 1.16.0, R package [21]. Default parameters and cell-specific size factors were computed by using the computeSumFactors function of the same package. The gene-by-cell count matrix of E2.5 sample was normalized by dividing the raw unique molecular identifier (UMI) counts by cell-specific size factors. The normalized counts were then log2-transformed by adding a pseudo-count of 1. One thousand highly variable genes (HVGs) in E2.5 PGCs were selected with respect to biological variability by using the decomposeVar and the getTopHVGs function of the scran package.

The *k*-nearest neighbor (kNN) graph was computed with FindNeighbors function of Seurat, version 3.1.5, R package [22] on the first 15 principal components (PCs) and used to compute clusters by using FindClusters function with resolution = 1.0. The 15 PCs were used to calculate uniform manifold approximation and projection (UMAP) by using RunUMAP function of the same package. Six clusters were identified, and a cluster of erythrocytes (which expressed genes such as *HBA1, HBAD, HBBA* and *HBBR*) was removed. For the remaining clusters, signature scores of the W-chromosome genes were calculated, and cluster with positive scores were annotated as female PGCs, whereas those with negative scores were annotated as male PGCs.

Count matrices of the samples (E2.5–1 w) for each sex were aggregated. Further normalization, HVG selection, dimensionality reduction, and clustering were performed as described above, with ten PCs of 434 HVGs for count matrix and resolution = 0.6 for males; and 750 HVGs, resolution = 0.6 for females. Clusters of putative doublets and low-quality cells were removed. The remaining cells were reclustered by using the method described above. Cell-cycle-specific clustering biases were regressed out during z-scaling of gene expression for the final 12 clusters of male samples and 16 clusters of female samples.

2.13. scRNA-seq data analysis of chicken germ cells

By calculating and clustering signature scores of Kyoto encyclopedia of genes and genomes (KEGG) gene sets, clusters from male germ cells were grouped into four developmental stages and those from females, into five stages. Differentially expressed genes (DEGs) of each stage were identified by using FindAllMarkers function of Seurat R package with default parameters. To identify biological processes enriched at each developmental stage, significantly upregulated or downregulated gene ontology biological process (GOBP) terms ($P < 0.05$) were selected with significant ($P < 0.05$) DEGs by using the topGO version 2.40.0, R package with the org.Gg.eg.db version 3.11.4, annotation data package.

Developmental trajectories of the chicken germ cells were estimated using the Palantir version 0.2.6, python package [23]. Diffusion components (DCs) were computed by using the run_diffusion_maps function of the package, with the first five PCs for males; and the first 20 for females. The kNN graph was constructed by using the first five DCs for males; and the first ten for females, and the cells were visualized on the t-SNE plot based on the same DCs. Starting cells for calculating pseudotime were defined by choosing the cell with the lowest expression of *FAP* (a cell-cycle-arrest-related gene) for male germ cells and the cell with the highest expression of *CXCR4* (a migration-related gene) for female germ cells. The pseudotime and branch probabilities of the trajectories were specified by using the run_palantir function of the Palantir python package with num_waypoints = 750. Female germ cells were assigned into one of two developmental fates by binomial sampling based on the calculated branch probabilities.

To calculate the transcription factor (TF) activities along pseudotime, chicken-specific TFs were retrieved from the AnimalTFDB3.0 [24]. Putative target genes for 485 TFs in males and 488 TFs in females were specified by using the algorithm for the reconstruction of accurate cellular networks with adaptive partitioning (ARACNe-AP) software [25]. Positively regulated target genes were identified using ssmarina, version 1.0.0, R package [26]. To calculate activity scores for the TF modules, the AUCell_calcAUC function of the AUCell version 1.10.0, R package [27] was used. The TF activities were smoothened over developmental pseudotime. They were hierarchically clustered by using the hclust function and visualized by heatmap.

To specify the bifurcation point of the developmental trajectories of female germ cells, the cells were ordered over pseudotime. Cells were grouped into 13 bins along the pseudotime. Eleven bins were defined to contain 1,002 cells each, and the remaining two bins were then assigned to contain 1,003 cells each. Pseudotime bins responsive to the developmental fates were prioritized on the basis of the cross-validation area under the receiver operating characteristic curve (AUC) of the random forest classifier implemented in the Augur, version 1.0.0, R package [28] with default parameters. DEGs between path 1 and path 2 cells after pseudotime bin 9 were identified by using the FindMarkers function of the Seurat R package.

2.14. Interspecies comparison of scRNA-seq data

The transcripts per kilobase million count tables of developing human gonadal cells were gathered from the NCBI GEO database (GSE86146) and log2-transformed. One thousand HVGs for males and 1000 for females were identified by using the methods described above. *DAZL*, *DDX4*, *DND1*, and *NANOG*-positive clusters from the gonad samples were annotated as fetal germ cells (FGCs) and were then extracted. Clustering and dimensionality reduction were done by using the methods described on 20 PCs, with resolution = 0.8. Then, eight identified clusters of male FGCs were grouped into three stages and eight clusters of female FGCs into four stages, by using the marker genes described by Li et al [29].

To compare development of chicken germ cells with that of human FGCs, 12,048 orthologs were identified for males and 12,009 orthologs were identified for females. For orthologous from male chicken germ cells (262 HVGs) and female chicken germ cells (565 HVGs), count matrices of chicken germ cells and human FGCs were extracted. The five chicken germ cells closest to each human FGC were identified by using the knn.index.dist function of the KernelKnn version 1.1.0, R package. The average of UMAP coordinates for the nearest neighbor were used to visualize chicken germ cells and human FGCs on a single scatter plot. Each human FGC was annotated as having the same developmental stage as that shared by most (three of five) of the closest chicken germ cells.

Developmental trajectories of human FGCs were estimated by using the Palantir python package [23]. DCs were computed by using the run_diffusion_maps function of the package, with the first 100 PCs for both males and females. The kNN graph was constructed by using the first 50 DCs for males and the first 25 DCs for females. Cells were visualized on the t-SNE plot based on the same DCs. Starting cells for calculating pseudotime were defined by choosing the cell with the highest expression of *POU5F1* (a pluripo-

tency and early-germ-cell marker) for both male and female germ cells. The pseudotime and branch probabilities of the trajectories were specified by using the run_palantir function of the Palantir python package with num_waypoints = 250. The dynamic expression pattern of intersection of HVGs for chicken germ cells and for human FGCs were smoothened over developmental pseudotime. The Z-scores were hierarchically clustered by using the hclust function and visualized by heatmap. Genes that showed convergent or divergent expression patterns were used to select GOBP terms ($P < 0.05$) by using the topGO, version 2.40.0, R package with the org.Hs.eg.db version 3.11.4, annotation data package.

3. Results

3.1. Genome editing to produce DAZL::GFP chicken PGCs

To trace PGCs during chicken development, we inserted *GFP* into the last intron of *DAZL* by using CRISPR/Cas9-NHEJ-mediated genome editing, as described [30]. First, we constructed a CRISPR/Cas9 plasmid to target the last intron of chicken *DAZL*, without affecting endogenous DAZL expression. Next, to tag *DAZL* with a GFP-expression cassette, we constructed a donor plasmid comprising portions of the last intron and exon (but not the stop codon) of *DAZL* (+12,099 to + 12,292) and a cassette to express GFP fused with the T2A self-cleavage peptide. The donor plasmid also included a neomycin-selection marker. To express GFP from the endogenous promoter of the modified *DAZL* allele, we transfected the constructed donor plasmid (including the gRNA-recognition sequences) and the CRISPR/Cas9 plasmid into chicken PGCs (Fig. 1A). Seven days after transfection, GFP expression was detected in several PGCs (Fig. 1B). GFP expression in PGCs was induced for an extended period after G418 drug selection (Fig. 1C). Flow cytometric analysis revealed that 70.7% of PGCs expressed GFP (Fig. 1D). We confirmed that we had tagged *DAZL* by using performing knock-in-specific PCR (Fig. 1E and Table S1). TA sequencing confirmed that the PGCs genomic DNA was edited by NHEJ, with and without indels (Fig. 1F).

The *DAZL::GFP* PGCs expressed normal levels of *DAZL* mRNA (as determined by RT-PCR and qRT-PCR) (Fig. 1G, H and Table S1) and DAZL protein (as determined by immunocytochemistry) (Fig. 1I). Besides, we examined the normal expression of candidate pluripotency marker genes (*POUV* and *NANOG*), PGC formation genes (*TBXT* and *PRDM14*), germ cell marker genes (*DDX4* and *PIWIL1*), epigenetic marker genes (*DNMT3B* and *HDAC3*), somatic marker gene (*SUZ12*), apoptosis marker gene (*FADD*), and DNA repair gene (*H2AFX*) in the *DAZL::GFP* PGCs by RT-PCR (Fig. 1J and Table S1). Among the examined genes, *POUV*, *NANOG*, *PRDM14*, *DDX4*, and *PIWIL1* are the *DAZL* interacting genes [31]. Also, the expression of *FADD* and *H2AFX* reinforces the previous report that the chicken PGCs express lower levels of apoptosis genes and higher levels of DNA repair genes [32]. These results indicate that the *DAZL::GFP* PGCs are a valuable resource to produce transgenic chickens by germline transmission.

3.2. Production of DAZL::GFP transgenic chickens by germline transmission

To test germline transmission of *DAZL::GFP* and to produce transgenic chickens, we transplanted genome-edited PGCs into Korean-Ogye-breed recipient embryos at HH stages 14–17. After the recipient males sexually matured, we confirmed donor-derived sperm and produced genome-edited progeny by test-cross analysis. In total, 24 donor-derived progeny (8.2%) were produced from one germline-chimeric chicken (#1066). Thirteen of these progeny (54.2%) had edited genomes (Table S2). We also identified genome-edited progeny (Fig. 2A) by using knock-in-specific PCR (Fig. 2B). Sequencing the amplicons from transgenic chicken revealed modified alleles either with or without indels at the junctions of exogenous and endogenous sequences (Fig. 2C). The transgenic chicken genotypes were identical to those of the genome-edited PGCs (Fig. 1F). To identify off-target effects, we sequenced eight off-target candidate genes in the transgenic chickens by TA cloning, which demonstrated no mutations in these selected genes (Table S3).

Next, we mated a transgenic male rooster (G1) with WT hens, and examined GFP expression at different embryonic stages in the ensuing progeny by using fluorescence microscopy. As expected, GFP expression was specifically detected in PGCs that migrated to the germinal crescent region at HH stage 4 (18–19 h of development) and thereafter in PGCs that settled in the embryonic gonads at HH stage 27 (E6). GFP was expressed in germ cells of both male and female embryonic gonads at HH stage 35 (E9) (Fig. 2D). Immunostaining of gonad sections of male and female transgenic chicken (at E6, E8, E12, E16, hatch, and 1 week post-hatch) to detect GFP expression in germ cells demonstrated, as expected, GFP expression in the male germ cells, which were pervasive in the early gonads (E6–E12) but restricted to the sex cords in the late gonads (E16–1 w). Similarly, we detected GFP expression in the female germ cells, which migrating to the cortex region of early gonads (E6) and which settled in the cortex region of the late gonads (E8–1 w) (Fig. 2E). These results indicate that the *DAZL::GFP* transgenic chicken model is valuable for tracing and isolating germ cells at various developmental times.

3.3. scRNA-seq reveals distinct developmental stages of chicken germ cells

To define developmental stages during chicken germ-cell development, we performed scRNA-seq of GFP^+ and PI^- *DAZL::GFP* germ cells isolated from transgenic chicken's blood circulation (at E2.5) and from gonads (at E6, E8, E12, E16, hatch, and 1 week post-hatch) (Fig. 3A and Table S4). We profiled 4,752 male and 13,028 female germ cells that had fulfilled our quality-control criteria (Table S4, Fig. S1A-C). Unsupervised graph-based clustering identified 12 clusters for male germ cells and 16 clusters for female germ cells, which were visualized by using UMAP plots (Fig. S1D). We classified clusters into four stages for male (mS1-mS4) germ cells and five stages for female (fS1-fS5) germ cells on the basis of cluster-specific signature scores of KEGG pathways (Fig. 3B, Fig. S1-D-F, Table S5). In males, each of these stages was enriched for cells at specific developmental time points. mS1 was enriched for cells at E2.5 and E6; mS2, for cells at E8 and E12; mS3, at E16 and hatch; and mS4, at 1 week post-hatch. Female germ cells at fS1 were enriched for cells at E2.5, E6, and E8; fS2, at E12; fS3, at E16 and hatch; fS4, at hatch and 1 week post-hatch; and fS5, at 1 week post-hatch (Fig. 3B). On the basis of the activated signature scores and the associated developmental time points of each stage, we annotated male stages as follows: mS1, migrating PGCs; mS2, mitotic gonocytes; mS3–mS4, mitotic-arrested prospermatogonia [7,33]. We annotated female stages as follows: fS1, migration to differentiating PGCs; fS2, mitotic to retinoic acid (RA)-responsive oogonia; fS3, RA-responsive to meiotic-arrest oocytes; fS4, meiotic-arrest to primordial-follicular oocytes; and fS5, primordial-follicular to growing-follicular oocytes [7,33–35].

In male germ cells, we observed that mS1 cells were distinguished by upregulation of focal-adhesion pathway, adherens-junction pathway, and Wnt-signaling pathway, which are important for PGC migration (Table S5) [36,37]. mS2 cells and mS3 cells were distinguished by upregulated Hedgehog-signaling pathway (which is involved in the mitotic phase in mS2 cells) [38] and steroid-biosynthesis pathway (which is related to cell-cycle arrest

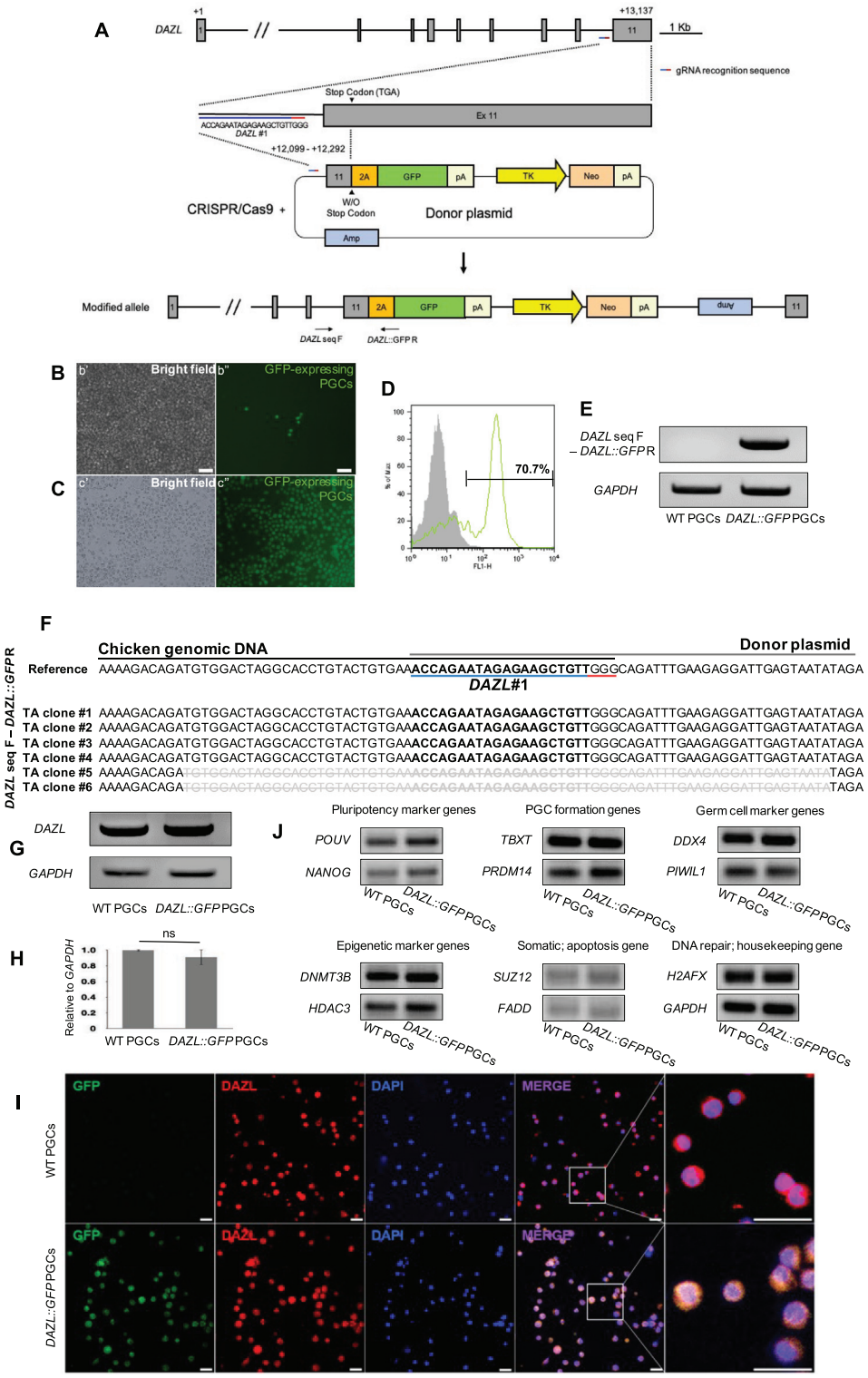

Fig. 1. CRISPR/Cas9-NHEJ-mediated genome editing to produce *DAZL::GFP* chicken primordial germ cells (PGCs). (A) CRISPR/Cas9 plasmid targeting the last intron of *DAZL* (*DAZL* #1) and donor plasmid containing the last intron and exon of *DAZL* (+12,099 to +12,292) in frame with a T2A peptide and green fluorescent protein (GFP) were cotransfected into cells to drive GFP expression from the endogenous *DAZL* promoter. Insertion did not disrupt the terminal *DAZL* exon. Blue bars indicate the gRNA-recognition sequence; red bars, the protospacer adjacent motif. (B–C) GFP expression in chicken PGCs seven days after transfection (b', b") and three weeks after transfection (c', c") with drug selection. (D) Flow cytometric analysis of genome-edited PGCs. (E–F) Analysis of targeted sites in chicken PGC genomes by using knock-in-specific PCR, and by sequencing TA-cloned amplicons. (G–H) Validation of endogenous *DAZL* mRNA expression by RT-PCR and qRT-PCR. In (H), the relative expression of *DAZL* was calculated by normalizing to both *GAPDH* expression and the control sample. Differences between samples were non-significant (ns), as determined by *t*-test. (I) Validation of endogenous DAZL protein expression via immunocytochemistry. (J) Examination of several candidate mRNA expression by RT-PCR. Wild-type (WT) PGCs were used as controls in (D, E, G, H, I, and J). Scale bars in (B, C, and I) = 100 μm. (For interpretation of the references to color in this figure legend, the reader is referred to the web version of this article.)

in mS3 cells) [39]. mS4 cells were distinguished by a strong transcriptional signature of the MAPK-signaling pathway, which is critical at different steps of male germ-cell development (including spermatogenesis, sperm maturation, and sperm activation) [40]. In female germ cells, we also found stage-specific activation of KEGG pathways (Table S5). fS1 cells were distinguished by activated Wnt- and TGFβ-signaling pathways, which are important for PGC proliferation and self-renewal [41,42]. fS2 cells (during oogonia development) were distinguished by activation of several DNA-repair pathways that maintain the genetic stability of germ cells [43,44] in the developing oogonia. fS3 cells were distinguished by activation of the MAPK-signaling pathway, which is in accord with the importance of RA for initiating meiosis in female germ cells [45,46]. fS4 cells had elevated G protein-coupled receptor-related sphingolipid-metabolism pathway, phosphatidylinositol-signaling pathway, and calcium-signaling pathway. These observations are in accord with the importance of both the G protein-coupled receptor-related pathway and calcium concentration for the meiotic-arrest phase in oocytes [47–49]. Finally, fS5 cells were enriched for pyruvate metabolism and steroid hormone biosynthesis, which are required for meiotic maturation and folliculogenesis [50,51].

To further characterize the molecular features of each stage, we identified stage-specific upregulated genes (adjusted $P < 0.05$; Fig. 3C and Table S6) and their enriched gene-ontology biological processes (Fig. 3D and Table S7). We found that heat-shock response gene expression was strongly enriched in mS1 and fS1 germ cells annotated as migrating PGCs, which is in line with the role of heat-shock proteins in the zebrafish PGC migration [52]. Gene sets involved in mitotic cell-cycle processes were upregulated in mS2 and fS2 cells and gene sets involved in meiosis were upregulated in fS4 cells. fS5 germ cells were enriched for expression of apoptosis-related genes (such as *BECN1*, *BNIP3*, *TOLLIP*, *ATG3*, and *ANXA7*) (Fig. S1G) [53–56]. We examined the expression (by qRT-PCR) of selected scRNA-seq-derived stage-specific markers in GFP-expressing germ cells: *LIN28A* for mS1 and fS1 germ cells; *KIF4B*, for mS2–mS3 cells; *TUBA3E*, for fS2–fS4 cells; *COL6A2*, for mS4 cells; and *ANXA7*, for fS5 cells (Fig. 3E, Table S1). We measured expression levels of several housekeeping genes to identify an appropriate normalization control. Although expression levels of commonly used housekeeping genes (including *GAPDH*) fluctuated over developmental stages (Fig. S2), we selected *SEC61B* (an essential factor for the embryonic development and protein trafficking in the oocyte of *Drosophila*) [57] for normalization. *SEC61B* expression was constant among developmental stages (Fig. S2).

In addition, we compared the transcriptomes of the mS1 and fS1 cells to provide insights into germ cell sex determination. Our analysis revealed that the mS1 and fS1 cells overlap at E2.5, E6, and E8 (Fig. S1A), however, the mS1 cells show a greater number of significantly upregulated genes (Fig. S3). Especially, genes related to sex determination (*SOX9*) [58], de novo DNA methylation (*DNMT3B*) [17], and PGCs migration (*CXCR4*) [59] were enriched in mS1 compared to fS1 (Table S8). Together, these data provide a temporal single-cell molecular atlas of gene expression during chicken germ-cell development and define the developmental stages of germ cells at a finer resolution.

3.4. Developmental trajectories and regulators mediating stage transition of chicken germ cells

We next investigated the developmental trajectories of male and female chicken germ cells by using Palantir [23]. We found that male germ cells linearly transitioned from mS1 to mS4. This trajectory was characterized by gradual acquisition of stage-specific TF activities (for example, during mS1, *SOX11*, *RCOR3*, *ARID3A*, *FOXN2*, *HLF*, and *ENSGALG00000021665*; during mS2, *TFDP2*, *MSX1*, and *ZNF521*; during mS3, *SMAD6* and *NR2C2*; and during mS4, *TFAP2D*, *IKZF1*, *ST18*, and *TWIST2*) (Fig. 4A-C, Table S9). Of the mS1-specific TFs, *SOX11* regulates progenitor- and stem-cell behavior during embryogenesis [60]; *RCOR3* epigenetically modulates the pluripotency-related gene *NANOG* in PGCs [61]; and *ARID3A* regulates different pluripotency genes (*OCT4*, *SOX2*, and *NANOG*) in embryonic stem cells [62]. These results reflect the pluripotent stem-cell characteristics of mS1 germ cells. The two TFs related to the BMP4-signaling pathway were activated at mS2 (*MSX1*) and mS3 (*SMAD6*). *MSX1* is critical for PGCs migration and proliferation [63]. *SMAD6* expression is lower in mouse gonocytes but higher in spermatogonia and spermatocytes [64], supporting our annotation of mS3 germ cells as mitotically arrested in a differentiated state.

By contrast, the trajectory of female germ cells bifurcated at fS3 (specifically at E16) to produce either a mixed population of fS4 and fS5 cells (path 1) or only fS4 cells (path 2) (Fig. 4A and B, Fig. S4). Along these bifurcating trajectories, we observed dynamic changes in stage-specific TF activities (such as in fS1, *EOMES* and *MSX1*; in fS2, *CSDE1*, *NCOR2*, *ZFHX3*, *ATF4*, *SSRP1*, *HMGB3*, and *GABPA*; in fS3, *DMRT1*; in fS4, *CERS6*, *SUB1*, *SIX6*, and *ARNTL2*; and in fS5, *GLIS1*) (Fig. 4C, Table S9). Of the fS1-specific TFs, *EOMES* is a stem-cell-related factor [65], and *MSX1* is critical for PGCs migration and proliferation [63]. These results suggest that the stem-cell characteristics of fS1 germ cells resemble those of mS1 cells. *MSX1* (which was also activated in mS2 cells) is also involved in meiosis initiation [66]. This suggests that whereas *MSX1* is involved in PGCs migration in both sexes, *MSX1* may specifically prepare female germ cells for early entry into meiosis. During chicken embryogenesis, female germ cells first enter meiosis, whereas male germ cells enter mitotic arrest [7,33]. Of the fS2-specific TFs, we found stem-cell-related factors (*CSDE1* and *GABPA*) [67] and oocyte-priming factor (*HMGB3*) [29], indicating asynchronous and heterogeneous germ-cell development. Furthermore, *HMGB3* (one of the top candidates for regulating the gene-expression network in the RA-responsive phase of human fetal germ cells [FGCs]) [29] was specifically expressed in fS2 cells. This indicated its involvement in both human and mouse oogenesis. The fS3-specific TF *DMRT1* is predominantly important for Sertoli-cell development and spermatogonia in the testis. However, *DMRT1* is also important for developing oogonia and oocytes (until meiosis entry) in the fetal ovary [68,69]. This indicates that the roles of *DMRT1* in male germ cells differ from those in female germ cells. Of the fS4-specific TFs, *SUB1* is one of the eight TFs essential to trigger oocyte growth at the transition from primordial to primary follicle. *SUB1* swiftly converts pluripotent stem cells into oocyte-like cells competent for fertilization and subsequent cleavage [70]. The fS5-specific *GLIS1*

Fig. 2. CRISPR/Cas9-NHEJ-mediated production and validation of *DAZL::GFP* transgenic chickens. (A) Donor-PGC-derived progeny were distinguished from WT chickens by feather color. (B–C) Representative results of knock-in-specific PCR of targeted sites, and sequencing of TA-cloned amplicons. (Blue and red bars are used as in Fig. 1.) The sequences of chicken genomic DNA and of the donor plasmid (including the terminal *DAZL* exon) are presented. A WT chicken was used as a control in (B). (D) GFP expression was observed (by using a fluorescence microscope) in PGCs migrating to the embryonic germinal crescent at HH stage 4 (18–19 h of development); PGCs settled in the embryonic gonads at HH stage 27 (Embryonic day [E] 6); and the germ cells of male and female embryonic gonads at HH stage 35 (E9). The fluorescence signal adjacent to the germinal crescent and gonadal regions was due to autofluorescence. (E) GFP expression was examined by immunohistochemistry in sections of male and female gonads at E6, E8, E12, E16, hatch, and 1 week post-hatch. Scale bars in (D) and (E) = 100 μm. (For interpretation of the references to color in this figure legend, the reader is referred to the web version of this article.)

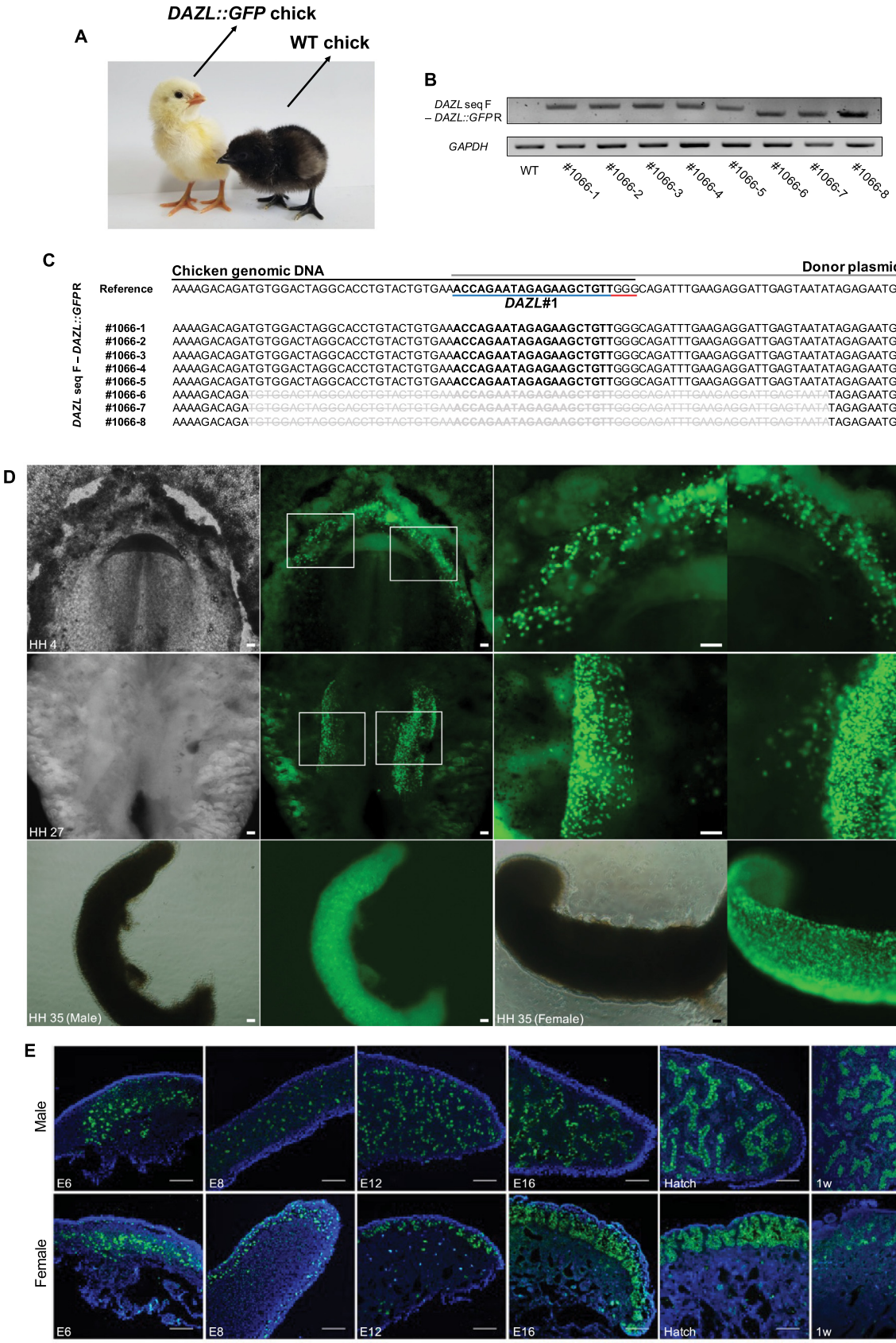
A
DAZL::GFP chick
WT chick
B
DAZL seq F – DAZL::GFP R
GAPDH
WT
#1066-1
#1066-2
#1066-3
#1066-4
#1066-5
#1066-6
#1066-7
#1066-8
C
Chicken genomic DNA
Donor plasmid
DAZL seq F – DAZL::GFP R
Reference AAAAGACAGATGTGGACTAGGCACCTGTACTGTGAAACCAGAATAGAGAAGCTGTTGGGCAGATTTGAAGAGGATTGAGTAATATAGAGAATGT
DAZL#1
#1066-1 AAAAGACAGATGTGGACTAGGCACCTGTACTGTGAAACCAGAATAGAGAAGCTGTTGGGCAGATTTGAAGAGGATTGAGTAATATAGAGAATGT
#1066-2 AAAAGACAGATGTGGACTAGGCACCTGTACTGTGAAACCAGAATAGAGAAGCTGTTGGGCAGATTTGAAGAGGATTGAGTAATATAGAGAATGT
#1066-3 AAAAGACAGATGTGGACTAGGCACCTGTACTGTGAAACCAGAATAGAGAAGCTGTTGGGCAGATTTGAAGAGGATTGAGTAATATAGAGAATGT
#1066-4 AAAAGACAGATGTGGACTAGGCACCTGTACTGTGAAACCAGAATAGAGAAGCTGTTGGGCAGATTTGAAGAGGATTGAGTAATATAGAGAATGT
#1066-5 AAAAGACAGATGTGGACTAGGCACCTGTACTGTGAAACCAGAATAGAGAAGCTGTTGGGCAGATTTGAAGAGGATTGAGTAATATAGAGAATGT
#1066-6 AAAAGACAGATGTGGACTAGGCACCTGTACTGTGAAACCAGAATAGAGAAGCTGTTGGGCAGATTTGAAGAGGATTGAGTAATATAGAGAATGT
#1066-7 AAAAGACAGATGTGGACTAGGCACCTGTACTGTGAAACCAGAATAGAGAAGCTGTTGGGCAGATTTGAAGAGGATTGAGTAATATAGAGAATGT
#1066-8 AAAAGACAGATGTGGACTAGGCACCTGTACTGTGAAACCAGAATAGAGAAGCTGTTGGGCAGATTTGAAGAGGATTGAGTAATATAGAGAATGT
D
HH 4
HH 27
HH 35 (Male)
HH 35 (Female)
E
Male
Female
E6
E8
E12
E16
Hatch
1w

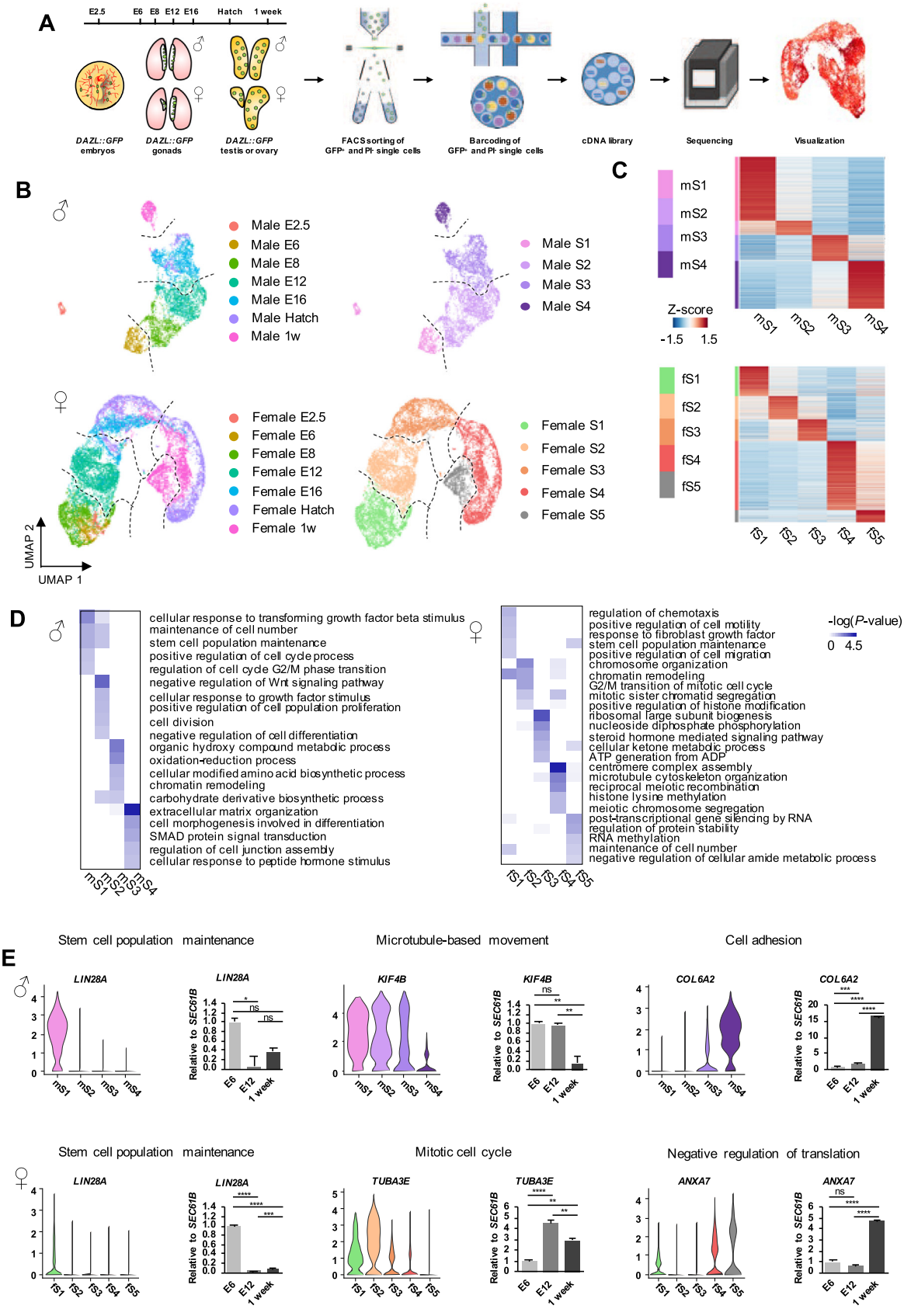
A
E2.5
E6
E8
E12
E16
Hatch
1 week
DAZL::GFP embryos
DAZL::GFP gonads
DAZL::GFP testis or ovary
FACS sorting of GFP+ and PI- single cells
Barcoding of GFP+ and PI- single cells
cDNA library
Sequencing
Visualization
B
Male E2.5
Male E6
Male E8
Male E12
Male E16
Male Hatch
Male 1w
Male S1
Male S2
Male S3
Male S4
Female E2.5
Female E6
Female E8
Female E12
Female E16
Female Hatch
Female 1w
Female S1
Female S2
Female S3
Female S4
Female S5
UMAP 2
UMAP 1
C
mS1
mS2
mS3
mS4
Z-score
-1.5
1.5
fS1
fS2
fS3
fS4
fS5
D
cellular response to transforming growth factor beta stimulus
maintenance of cell number
stem cell population maintenance
positive regulation of cell cycle process
regulation of cell cycle G2/M phase transition
negative regulation of Wnt signaling pathway
cellular response to growth factor stimulus
positive regulation of cell population proliferation
cell division
negative regulation of cell differentiation
organic hydroxy compound metabolic process
oxidation-reduction process
cellular modified amino acid biosynthetic process
chromatin remodeling
carbohydrate derivative biosynthetic process
extracellular matrix organization
cell morphogenesis involved in differentiation
SMAD protein signal transduction
regulation of cell junction assembly
cellular response to peptide hormone stimulus
regulation of chemotaxis
positive regulation of cell motility
response to fibroblast growth factor
stem cell population maintenance
positive regulation of cell migration
chromosome organization
chromatin remodeling
G2/M transition of mitotic cell cycle
mitotic sister chromatid segregation
positive regulation of histone modification
ribosomal large subunit biogenesis
nucleoside diphosphate phosphorylation
steroid hormone mediated signaling pathway
cellular ketone metabolic process
ATP generation from ADP
centromere complex assembly
microtubule cytoskeleton organization
reciprocal meiotic recombination
histone lysine methylation
meiotic chromosome segregation
post-transcriptional gene silencing by RNA
regulation of protein stability
RNA methylation
maintenance of cell number
negative regulation of cellular amide metabolic process
-log(P-value)
0
4.5
E
Stem cell population maintenance
Microtubule-based movement
Cell adhesion
LIN28A
KIF4B
COL6A2
SEC61B
Relative to
E6
E12
1 week
Stem cell population maintenance
Mitotic cell cycle
Negative regulation of translation
TUBA3E
ANXA7

is a maternal TF enriched in oocytes and one-cell-stage embryos. *GLIS1* effectively and directly promotes reprogramming of somatic cells into induced pluripotent stem cells (iPSC) [71]. Moreover, chicken oocytes store maternal factors (including TFs) for zygotic genome activation and specification of the next generation of PGCs [72].

In the female germ cells, the bifurcating trajectories (paths 1 and 2) were distinguished by mutually exclusive patterns of gene expression. These cells developing along path 1 expressed genes related to apoptosis (*ACTB*, *MAPK8*, and *ATF4*) [73–75]; and those along path 2, meiosis (*RBX1*, *CALM2*, and *ANAPC10*) [76–78]. This observation supported our annotation of these two stages (Fig. 4D and E, Table S10). Moreover, we examined the expression (by qRT-PCR) of above apoptosis and meiosis-related genes in the *DAZL::GFP* germ cells isolated from the E16, hatch, and 1 week post-hatch ovaries (Fig. 4E). PGCs, oogonia, and oocytes apoptose at various stages of mammalian meiosis. However, a substantial proportion of oocyte apoptosis occurs during meiotic prophase I (mainly at the zygotene/pachytene stage) in the fetal and early postnatal ovaries (before follicle formation) [79]. Oocytes may apoptose at this stage because of limited levels of growth factors necessary for oocyte survival and because of defects in chromosome crossover [79,80]. Moreover, oocyte apoptosis occurs in fetal and early postnatal ovaries because of the breakdown of germ-cell cysts and the formation of primordial follicles [81]. Although there is no evidence of this in chickens, our results are consistent with these observations in mammalian fetal and early postnatal ovaries.

To provide further insight into oocyte meiosis, we first analyzed the expression patterns of candidate meiosis initiators in the chicken female germ cells developing along path 2. Our analysis revealed that the meiosis initiators *PLCB1*, *MSX1*, and *RDH10* express in a population of fS1 (Fig. 5A), earlier than the previously known pre-meiotic marker *STRA8*, which is triggered by retinoic acid and essential for the initiation of meiosis [34]. Next, we sub-clustered the fS3-fS5 cells and analyzed the expression patterns of candidate meiotic prophase I markers. Our analysis revealed 14 sub-clusters in fS3-fS5 (Fig. 5B). By the expression of meiotic prophase I markers, *SPO11* (leptotene marker), *RAD21L1* (zygotene marker), and *PIWIL1* (pachytene marker) were particularly expressed relatively high in sub-clusters 4, 6, 9, 10, and 13 (mostly fS3-fS4 cells) (Fig. 5B-C), indicating the accumulation of meiotic-arrested oocytes at these stages. After entry into meiosis, oocytes are usually arrested in the meiotic prophase I and maintained in the primordial follicles, which forms within few days after hatch in chicken [35]. We have also examined (by qRT-PCR) the expression of *MSX1*, *SPO11*, and *RAD21L1* in the *DAZL::GFP* germ cells isolated from the E12, E16, and hatch ovaries (Fig. 5D). Finally, we sub-clustered the fS5 cells and checked the expression patterns of genes related to apoptosis (*ACTB*, *MAPK8* and *ATF4*) and meiosis (*RBX1*, *CALM2* and *ANAPC10*). We found that the subpopulation structure of fS5 cells is largely explained by the expression of *MAPK8* (Fig. 5E-F). Together, these results identify stage-specific TF activities that govern the progression of chicken germ cells through developmental stages and that define the path of oocyte meiosis and apoptosis at a finer resolution.

3.5. Comparison of chicken and human germ-cell stages reveals species-specific gene expression

To determine whether the developmental stages and trajectories of chicken germ cells resemble those of human FGCs [29], we compared scRNA-seq data from these cell types by clustering gene expression of male FGCs (4–25 w after fertilization) and female FGCs (5–26 w after fertilization) and using the clusters to define three developmental stages in male cells and four stages in female cells (Fig. 6A, Fig. S5A and S5B). We mapped the human FGCs data onto the chicken germ-cell data, and mapped the chicken germ-cell data onto the human FGC data. For males, we mapped human mS1 to chicken mS1; human mS2 to chicken mS2; and human mS3 to chicken mS2–mS4. For females, we mapped human fS1 to chicken fS1; human fS2 to chicken fS2–fS4; human fS3–fS4 to chicken fS4 (Fig. 6B and C, Fig. S6A-C, Table S11).

We then compared the inferred developmental trajectories of human FGCs with those of chicken germ cells by manually inspecting expression dynamics in each species. In males, of 56 orthologs dynamically expressed along the human or chicken trajectories, we identified 32 convergent (evolutionary conserved) and 24 divergent (species-specific) genes. In females, we identified 83 convergent and 36 divergent genes (Fig. 6D, Table S12). The convergent and divergent genes in both sexes were significantly enriched for various cell-cycle-related functions, reflecting the fact that proliferation is essential for germ-cell development. As expected, female-specific convergent and divergent genes were additionally enriched for meiosis-related functions (Table S13).

To add further insight into the germ cell biology between the chicken and humans, we endeavored to find out the general germ-cell-specific genes and germ-plasm-specific genes among the convergent and divergent genes. Even though most germ-cell-specific genes were not dynamically expressed along the male trajectory, *TCF7L2* (a mitotic-arrest related gene) [82] was identified as a divergent gene (Fig. 6D). We also identified female-specific convergent genes associated with pluripotency, germ-cell development, and meiosis (including *SALL4*, *KIT*, *SPO11*, *SYCP1*, *SYCP2* and *SYCE3*) (Fig. 6D) [33,83–86]. *DDX4* and *DAZL* are well-known germ-cell-specific as well as germ-plasm-specific marker genes in chicken [3,4]. In our analysis of germplasm genes, *DDX4* and *TDRKH* (which is not well-known in chicken) were identified as divergent genes in the male germ cells between chicken and human, while *DDX4* and *DAZL* were identified as divergent genes in the female germ cells between the species. Most of the other germplasm genes, including *MAEL*, were identified as convergent genes in both male and female germ cells between the species (Fig. 6E). Some of the chicken germ-plasm-specific genes, including *DAZL*, are not required for the specification and migration of PGCs in mammals since the mammals follow epigenesis mode of germ cells specification, whereas chickens follow preformation mode of germ cells specification [2,87]. Together, these comparisons of human-gene expression with chicken-gene expression during germ-cell development identified several evolutionarily conserved cell-cycle-related functions and diverse species-specific biological processes.

Fig. 3. Transcriptional landscape of chicken germ cells. (A) Workflow of the scRNA-seq analysis of *DAZL::GFP* transgenic chicken germ cells. (B) Uniform manifold approximation and projection (UMAP) plot showing expression in male (top) and female (bottom) germ cells. Cells were colored by elapsed time of development (left) and by developmental stage (right). (C) Heatmaps illustrating average Z-scores of stage-specific differentially expressed genes (DEGs) for each stage of male (top) and female (bottom) germ cells. (D) Heatmaps displaying the enriched gene ontology biological process (GOBP) terms ($P < 0.05$) for each stage from the male (left) and female (right) germ-cell stages. (E) Violin plots showing expression levels of candidate stage-specific genes for male (top) and female (bottom) germ-cell stages calculated from scRNA-seq data; bar plots showing normalized expression of the same genes examined by qRT-PCR. For qRT-PCR analysis, the relative expression of genes was calculated by normalizing to the expression of a housekeeping gene (*SEC61B*) and reference sample, and one-way ANOVA with Tukey's multiple comparisons test was applied to calculate statistical significance. * $P < 0.05$, ** $P < 0.01$, *** $P < 0.001$, **** $P < 0.0001$, ns – no significant difference. (For interpretation of the references to color in this figure legend, the reader is referred to the web version of this article.)

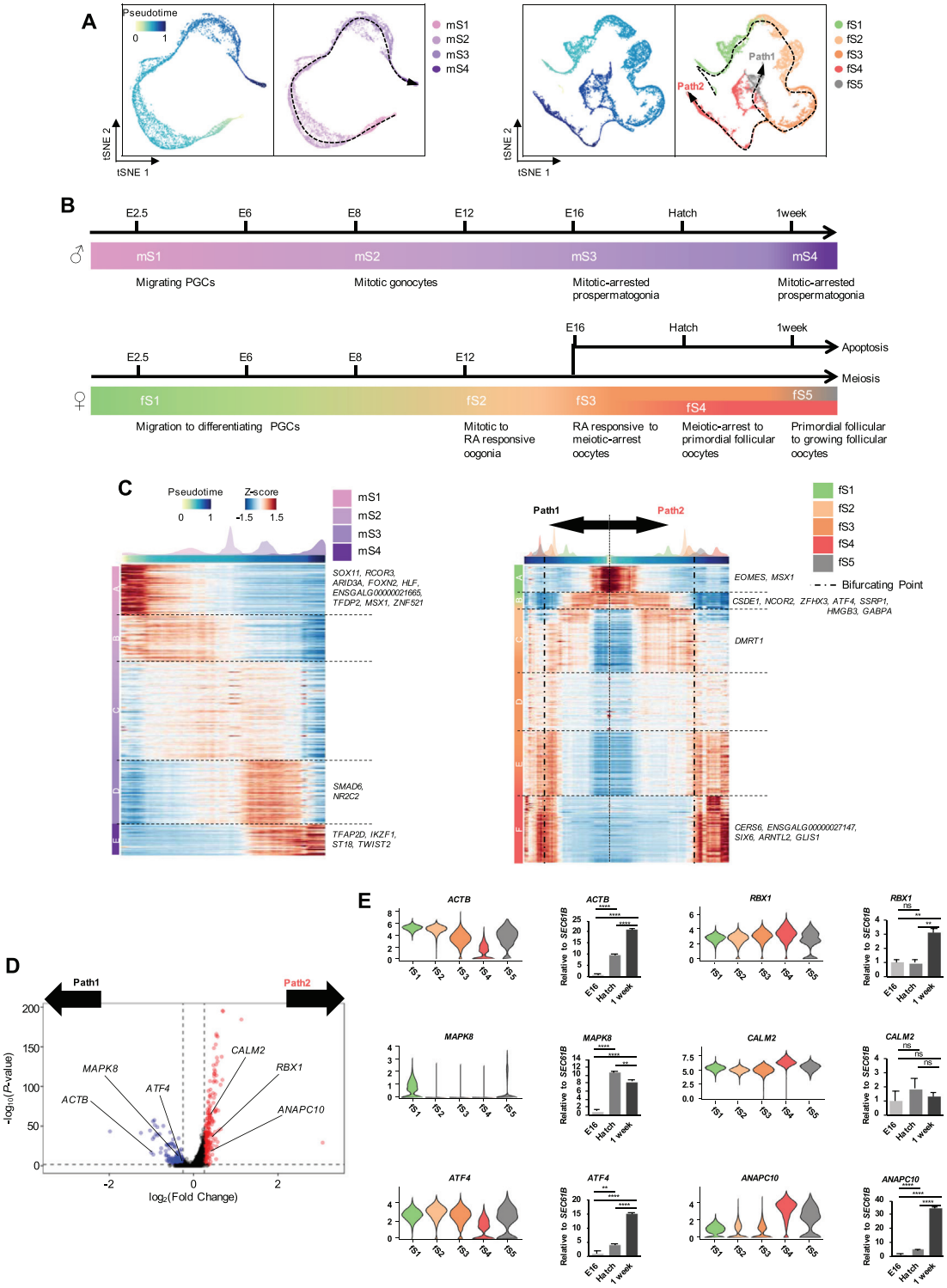

Fig. 4. Developmental trajectories and regulators that mediate chicken germ-cell transitions between stages. (A) t-SNE plot showing the developmental pseudotime and annotated stages of male (left) and female (right) germ cells. Cells are colored by calculated pseudotime and by stages. (B) Schematic of developmental time points, stages, and trajectories of germ cells. (C) Heatmaps displaying the stage-specific transcription factor (TF) activities over the calculated pseudotimes for male (left) and female (right) germ cells. The dotted lines segment TFs active in specific stages. Histogram above the heatmaps showing the cell density of each developmental stage in male and female germ cells, respectively. The alphabet on the left side of the heatmaps indicate the cluster of the genes with similar dynamic expression patterns along pseudotime. (D) Volcano plot illustrating the DEGs between developmental path 1 and path 2 of female germ cells. Blue dots indicate genes upregulated in path 1; red dots, in path 2. (E) Violin plots showing the expression levels of apoptosis pathway genes enriched in path 1 (left) and of meiosis-pathway genes enriched in path 2 (right) in female germ cells calculated from scRNA-seq data; bar plots showing normalized expression of the same genes examined by qRT-PCR. For qRT-PCR analysis, the relative expression of genes was calculated by normalizing to the expression of *SEC61B* and reference sample, and one-way ANOVA with Tukey's multiple comparisons test was applied to calculate statistical significance. ** $P < 0.01$, **** $P < 0.0001$, ns – no significant difference. (For interpretation of the references to color in this figure legend, the reader is referred to the web version of this article.)

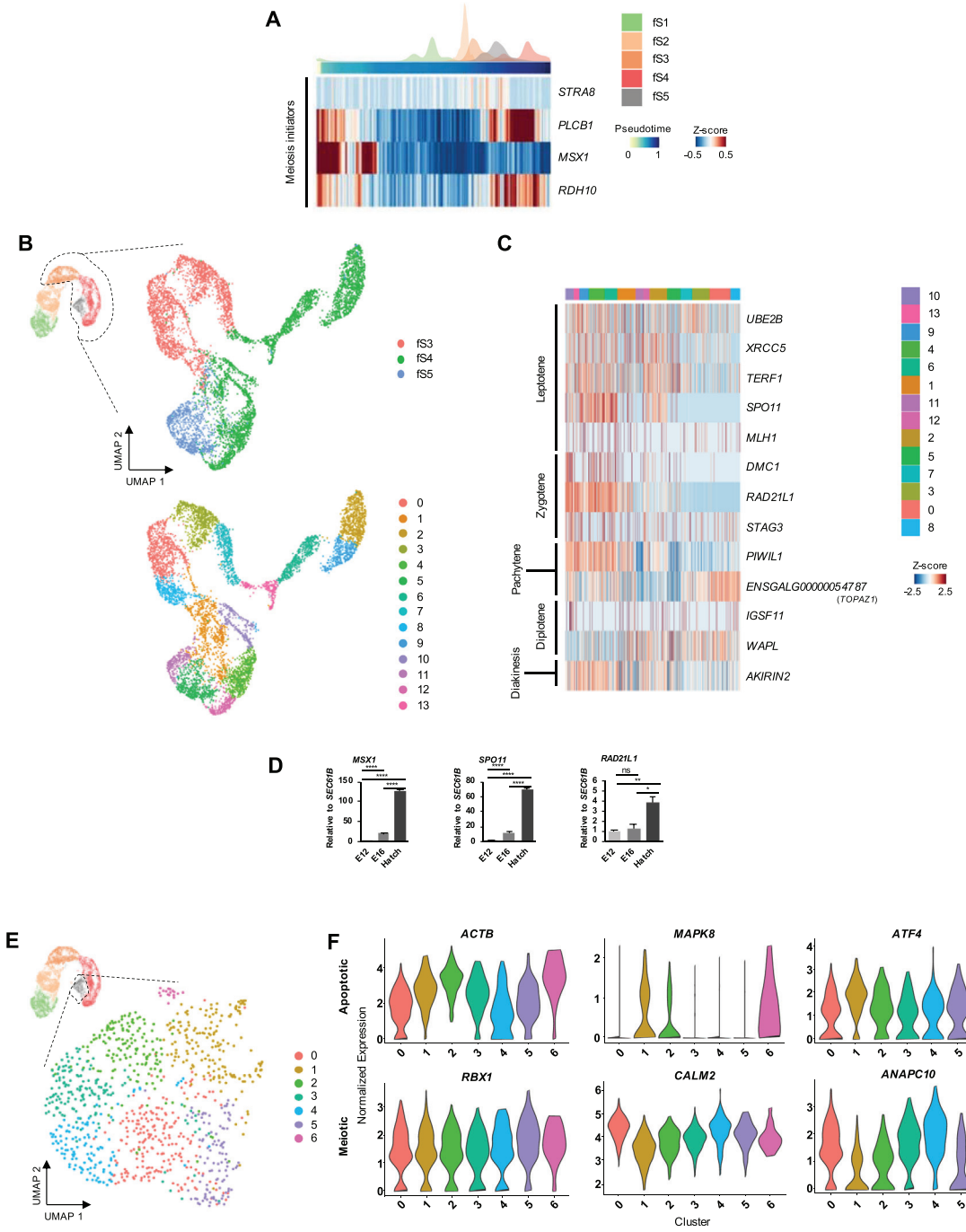

Fig. 5. Expression patterns of meiosis initiators and meiotic prophase I markers in the chicken female germ cells developing along path 2. (A) Heatmap displaying the dynamic expression patterns of meiosis initiators over the calculated pseudotime. Histogram above the heatmap showing the cell density of each developmental stages in female germ cells. (B) UMAP of female S3-S5 cell subset. Colors indicate the assigned stages (top) or assigned cluster after graph-based unsupervised clustering (bottom). (C) Heatmap displaying the expression patterns of meiotic prophase I markers in female S3-S5 sub-clusters. (D) Bar plots showing normalized expression of the candidate meiosis genes examined by qRT-PCR. For qRT-PCR analysis, the relative expression of genes was calculated by normalizing to the expression of *SEC61B* and reference sample, and one-way ANOVA with Tukey's multiple comparisons test was applied to calculate statistical significance. * $P < 0.05$, ** $P < 0.01$, **** $P < 0.0001$, ns – no significant difference. (E) UMAP of female S5 cell subset. Cells are colored with their assigned clusters after graph-based unsupervised clustering. (F) Violin Plots for the normalized expression of apoptotic and meiotic genes in female S5 sub-clusters. (For interpretation of the references to color in this figure legend, the reader is referred to the web version of this article.)

4. Discussion and conclusion

Transcriptome analyses of chicken germ-cell developmental stages have been limited and fragmentary [31,88], and these analyses have not been applied *in vivo*. The main reasons for these limitations are the lack of a technology to discriminate germ cells and the lack of sophisticated markers to isolate these cells. Recently, scRNA-seq was used to compare undifferentiated germ cells with somatic cells; as well as to compare germ cells at different stages of sexual maturation [89–93]. In this study, we used scRNA-seq to produce a single-cell-resolution atlas of the dynamic transcriptional landscape during chicken germ-cell

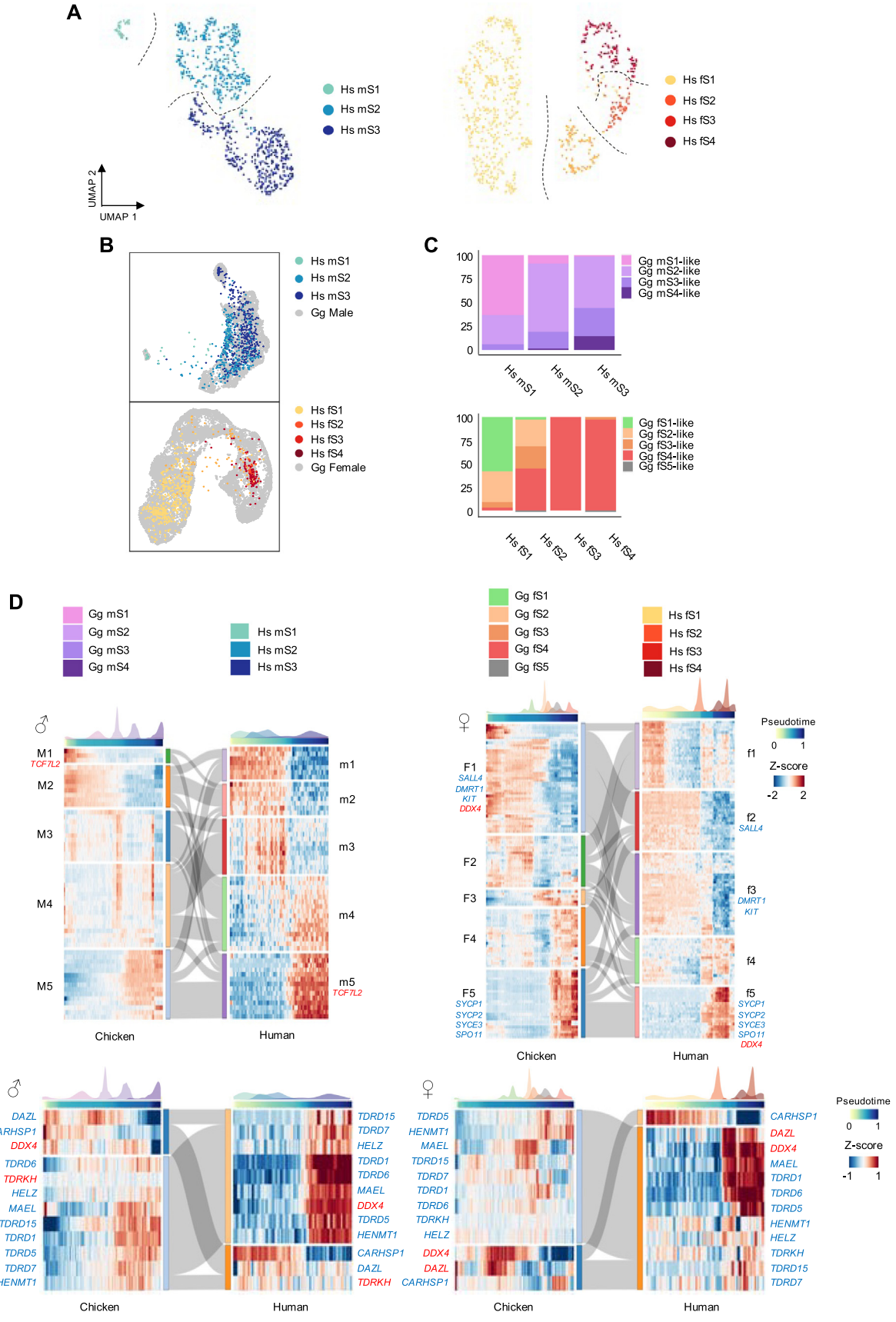
A
Hs mS1
Hs mS2
Hs mS3
Hs fS1
Hs fS2
Hs fS3
Hs fS4
UMAP 2
UMAP 1
B
Hs mS1
Hs mS2
Hs mS3
Gg Male
Hs fS1
Hs fS2
Hs fS3
Hs fS4
Gg Female
C
Gg mS1-like
Gg mS2-like
Gg mS3-like
Gg mS4-like
Hs mS1
Hs mS2
Hs mS3
Gg fS1-like
Gg fS2-like
Gg fS3-like
Gg fS4-like
Gg fS5-like
Hs fS1
Hs fS2
Hs fS3
Hs fS4
D
Gg mS1
Gg mS2
Gg mS3
Gg mS4
Hs mS1
Hs mS2
Hs mS3
M1
TCF7L2
M2
M3
M4
M5
m1
m2
m3
m4
m5
TCF7L2
Chicken
Human
Gg fS1
Gg fS2
Gg fS3
Gg fS4
Gg fS5
Hs fS1
Hs fS2
Hs fS3
Hs fS4
Pseudotime
Z-score
F1
SALL4
DMRT1
KIT
DDX4
F2
F3
F4
F5
SYCP1
SYCP2
SYCE3
SPO11
f1
f2
SALL4
f3
DMRT1
KIT
f4
f5
SYCP1
SYCP2
SYCE3
SPO11
DDX4
Chicken
Human
E
DAZL
CARHSP1
DDX4
TDRD6
TDRKH
HELZ
MAEL
TDRD15
TDRD1
TDRD5
TDRD7
HENMT1
TDRD15
TDRD7
HELZ
TDRD1
TDRD6
MAEL
DDX4
TDRD5
HENMT1
CARHSP1
DAZL
TDRKH
Chicken
Human
TDRD5
HENMT1
MAEL
TDRD15
TDRD7
TDRD1
TDRD6
TDRKH
HELZ
DDX4
DAZL
CARHSP1
CARHSP1
DAZL
DDX4
MAEL
TDRD1
TDRD6
TDRD5
HENMT1
HELZ
TDRKH
TDRD15
TDRD7
Chicken
Human
Pseudotime
Z-score

development (from undifferentiated to differentiated stages) in both sexes.

We developed a strategy to monitor and isolate chicken germ cells by inserting *GFP* into *DAZL* (a germ-cell-specific gene). Adopting a published method [94], we inserted a *T2A-GFP* cassette in frame with the last exon of *DAZL* by using CRISPR/Cas9. Successful editing was confirmed by monitoring GFP expression in the established PGC lines (*DAZL::GFP*) and no alteration of endogenous *DAZL* expression was observed. *DAZL::GFP* transgenic chickens were produced by transplanting *DAZL::GFP* PGC lines, indicating that genome-edited PGCs can be transmitted through the germline. Furthermore, in G2 embryos of transgenic chickens, we detected GFP expression specifically in germ cells of both sexes at HH stages 4, 27, and 35. These results indicate that these transgenic chickens are useful for monitoring germ-cell development. By isolating germ cells for scRNA-seq analyses, we could also characterize germ-cell-specific mechanisms during avian development. Thus, the CRISPR/Cas9-NHEJ-mediated gene-insertion strategy is a powerful method to edit chicken genomes and to reveal tissue-specific gene expression patterns in both avian and mouse models [95].

Using our method, we identified several cellular and molecular characteristics of germ-cell development in both sexes. Male germ cells were characterized into four developmental stages (mS1, migration stage; mS2, mitotic stage; mS3–mS4, mitotic-arrest stages), according to activated signature scores and the elapsed time of development [7,33]. Sometimes, female germ cells (particularly those in fS1–fS4) were classified simultaneously into multiple adjacent stages, indicating that germ-cell development in females is asynchronous and heterogeneous [7,29,33,35]. These results indicate that (in chickens) the development of female germ cells is more advanced than that of male germ cells and that many female germ cells are in states of transition. We identified LIN28A as an mS1 and fS1 marker. LIN28A is essential for proper PGC development [96], and LIN28A induces somatic cells to become PGCs [97]. Previous studies have attempted to distinguish the phenotypes of E2.5 PGCs from E6 PGCs [98,99], however, the transcriptomic difference has not been clearly identified. We found that the expression profiles of migrating PGCs (at E2.5) resemble those of colonized PGCs (at E6 in males and at E6–E8 in females). In mice, it is known that the transcriptomes of XX and XY cells overlap at the early developmental stage, whereas sex-specific branches are formed in the differentiated cells at the late stages [100]. However, in this study, chickens showed differences in transcriptome levels between mS1 and fS1 (early-stage germ cells).

We found that the gene-expression profiles of male germ cells differed from those of female germ cells after E8 (which corresponds to mS2 in male germ cells, and to fS1 in females). After E8, the number of mitotic male germ cells rapidly declined, and most cells begin to arrest at G0/G1 of mitosis [7]. Reflecting this phenomenon, the transcriptional signatures of cell division, of cellular response to growth factor stimulus, and of positive regulation of cell population proliferation were elevated in mS2 cells but not in mS3 cells. On the other hand, after E8 the female germ cells rapidly proliferated and begin to arrest at G2/M of meiosis [7]. Consistent with this, we observed that the G2/M transition was regulated and that fS2 cells actively divided during meiosis. These transcriptional signatures persisted into fS3, but did not persist into fS4 and fS5. Our analysis shows that the trajectory of female germ-cell development, particularly after fS3 (E16), bifurcates to produce apoptotic cells (from path 1) and meiotic cells (from path 2). In mammals, a substantial proportion of oocyte apoptosis occurs throughout meiotic prophase I in fetal and early postnatal ovaries. This is mainly because of limited levels of growth factors necessary for oocyte survival and because of elimination of oocytes with chromosome-crossover defects [79,80]. Also, the environment of ovaries before birth differs from that after birth (in relation to the breakdown of germ-cell cysts and the formation of primordial follicles). When the mouse cysts undergo programmed breakdown in the fetal ovary, approximately 33% of the oocytes survive to form primordial follicles [81]. We found that fS4–fS5 germ cells developing along path 1 were apoptotic. In chickens, the primordial follicle pool begins to develop within 4 days of hatch by germ-cell cysts breakdown and by enclosure of oocytes with pregranulosa cells [35].

A comparison of chicken germ cells with human FGCs [29] revealed sexually dimorphic similarities and differences. On the one hand, we matched the first two stages of human male FGC development (mS1 and mS2) with the first two stages of chicken male germ-cell development (mS1 and mS2). In later stages as well, the gene expression profiles of human male FGCs and chicken male germ cells were very similar. On the other hand, in females, the human fS2 stage matched with a broad range of chicken germ-cell stages (fS2–fS4). The similarity between human FGC and chicken germ-cell transcriptomes was lower in females than in males. Based on these results, further in-depth analyses of chicken germ-cell characteristics at each stage and of interactions between germ cells and somatic cells are required. In conclusion, we used a novel method to trace germ cells and to produce a time-resolved single-cell-resolution atlas of chicken germ-cell development. Our results highlight the cellular and molecular characteristics of different stages in germ-cell development. These results could be valuable for using chicken as a model system to study germ-cell development.

Declaration of Competing Interest

The authors declare that they have no known competing financial interests or personal relationships that could have appeared to influence the work reported in this paper.

Acknowledgments

This work was supported by grants: J.Y.H. (National Research Foundation of Korea grant [NRF-2015R1A3A2033826] funded by the Ministry of Science, Information and Communication Technology, and Future Planning), J.K.K. (2018R1A5A1025511 and DGIST R&D program [20-CoE-BT-04] funded by the Ministry of Science and ICT of Korea), and H.J.L. (National Research Foundation of Korea grant [NRF-2018R1D1A1B07048893] funded by the Ministry of Education).

Fig. 6. Transcriptome-based comparison of developmental stages in chicken germ cells with those in human fetal germ cells (FGCs). (A) UMAP showing the developmental stages of human male (left) and female (right) FGCs. Cells are colored by developmental stage. (B) Scatter plots mapping human male FGCs onto the UMAP plot of chicken male germ cells (top); and human female FGCs onto chicken female germ cells (bottom). Gray points indicate chicken germ cells; colored points, original developmental stages of human FGCs. (C) Bar plots showing proportions of human FGCs in different stages that were mapped onto chicken germ-cell stages, corresponding to (B). (D) Heatmaps showing dynamic patterns of DEGs from chicken male germ cells and human male FGCs (left); and from chicken female germ cells and human female FGCs (right). (E) Heatmaps showing dynamic patterns of germ-plasm-specific genes from chicken male germ cells and human male FGCs (left); and from chicken female germ cells and human female FGCs (right). In D and E, histogram above the heatmaps showing the cell density of each developmental stages in male and female germ cells, and in each species, respectively. Gray lines between gene clusters connect chicken and human orthologs. Notable convergent (blue) and divergent (red) genes are indicated. Gg, *Gallus gallus* (chicken); Hs, *Homo sapiens* (human). (For interpretation of the references to color in this figure legend, the reader is referred to the web version of this article.)

Author Statement

Deivendran Rengaraj, Dong Gon Cha, Hong Jo Lee, and Young Min Kim analyzed the scRNA-seq data, investigated the results, and wrote the first draft of manuscript. Deivendran Rengaraj, Hong Jo Lee, Kyung Youn Lee, and Yoon Ha Choi prepared single-cells and libraries for scRNA-seq. Hong Jo Lee, Deivendran Rengaraj, Kyung Youn Lee, Kyung Min Jung, Young Min Kim, and Hee Jung Choi contributed to producing transgenic chickens and performed the experiments. Hyeon Jeong Choi, Eunhui Yoo, Seung Je Woo, Jin Se Park, and Kyung Je Park assisted in animal management, sample preparation, scRNA-seq data analysis and experiments. Jae Yong Han and Jong Kyoung Kim conceived the project, supplied research materials, investigated the results, and critically checked the content in the draft. All authors have read and agreed to the published version of the manuscript.

Data and code availability

The single-cell RNA sequencing data have been deposited in the SRA database under the accession code PRJNA761874 and are available. The scripts and instances used for the analysis of the single-cell RNA sequencing data are uploaded in the GitHub: https://github.com/CB-postech/Chicken_GermCell. The source data underlying gel electrophoresis images and qRT-PCR are provided as a Source Data file with this paper.

Ethics approval

All experimental procedures and care of chickens were approved by the Institute of Laboratory Animal Resources, Seoul National University, Korea, and all methods were carried out in accordance with ARRIVE (Animal Research: Reporting of In Vivo Experiments) guidelines and approved by the Institutional Animal Care and Use Committee (IACUC, SNU-190401-1-1) of Seoul National University, Korea.

Consent to participate

Not applicable.

Consent for publication

Not applicable.

Appendix A. Supplementary data

Supplementary data (Figures and Tables) to this article can be found online at https://doi.org/10.1016/j.csbj.2022.03.040.

References

[1] Kim YM, Han JY. The early development of germ cells in chicken. Int J Dev Biol 2018;62:145–52.
[2] Jamieson-Lucy A, Mullins MC. The vertebrate Balbiani body, germ plasm, and oocyte polarity. Curr Top Dev Biol 2019;135:1–34.
[3] Tsunekawa N, Naito M, Sakai Y, et al. Isolation of chicken vasa homolog gene and tracing the origin of primordial germ cells. Development 2000;127:2741–50.
[4] Lee HC, Choi HJ, Lee HG, et al. DAZL expression explains origin and central formation of primordial germ cells in chickens. Stem Cells Dev 2016;25:68–79.
[5] Eyal-Giladi H, Kochav S. From cleavage to primitive streak formation: a complementary normal table and a new look at the first stages of the development of the chick. I General morphology. Dev Biol 1976;49:321–37.
[6] Hamburger V, Hamilton HL. A series of normal stages in the development of the chick embryo. J Morphol 1951;88:49–92.
[7] Yang SY, Lee HJ, Lee HC, et al. The dynamic development of germ cells during chicken embryogenesis. Poult Sci 2018;97:650–7.
[8] Western PS, Miles DC, van den Bergen JA, et al. Dynamic regulation of mitotic arrest in fetal male germ cells. Stem Cells 2008;26:339–47.
[9] Miles DC, van den Bergen JA, Sinclair AH, et al. Regulation of the female mouse germ cell cycle during entry into meiosis. Cell Cycle 2010;9:408–18.
[10] Hughes GC. The population of germ cells in the developing female chick. J Embryol Exp Morphol 1963;11:513–36.
[11] Méndez C, Carrasco E, Pedernera E. Adenohypophysis regulates cell proliferation in the gonads of the developing chick embryo. J Exp Zool A Comp Exp Biol 2005;303:179–85.
[12] Nakamura Y, Yamamoto Y, Usui F, et al. Migration and proliferation of primordial germ cells in the early chicken embryo. Poult Sci 2007;86:2182–93.
[13] Li H, Liang Z, Yang J, et al. DAZL is a master translational regulator of murine spermatogenesis. Natl Sci Rev 2019;6:455–68.
[14] Rengaraj D, Zheng YH, Kang KS, et al. Conserved expression pattern of chicken DAZL in primordial germ cells and germ-line cells. Theriogenology 2010;74:765–76.
[15] Sakuma T, Nishikawa A, Kume S, et al. Multiplex genome engineering in human cells using all-in-one CRISPR/Cas9 vector system. Sci Rep 2014;4:5400.
[16] Han JY, Park TS, Kim JN, et al. Gene expression profiling of chicken primordial germ cell ESTs. BMC Genomics 2006;7:220.
[17] Rengaraj D, Lee BR, Lee SI, et al. Expression patterns and miRNA regulation of DNA methyltransferases in chicken primordial germ cells. PLoS ONE 2011;6:e19524.
[18] Dobin A, Davis CA, Schlesinger F, et al. STAR: ultrafast universal RNA-seq aligner. Bioinformatics 2013;29:15–21.
[19] Lun ATL, Riesenfeld S, Andrews T, et al. EmptyDrops: distinguishing cells from empty droplets in droplet-based single-cell RNA sequencing data. Genome Biol 2019;20:63.
[20] McCarthy DJ, Campbell KR, Lun AT, et al. Scater: pre-processing, quality control, normalization and visualization of single-cell RNA-seq data in R. Bioinformatics 2017;33:1179–86.
[21] Lun AT, McCarthy DJ, Marioni JC. A step-by-step workflow for low-level analysis of single-cell RNA-seq data with Bioconductor. F1000research 2016;5:2122.
[22] Satija R, Farrell JA, Gennert D, et al. Spatial reconstruction of single-cell gene expression data. Nat Biotechnol 2015;33:495–502.
[23] Setty M, Kiseliovas V, Levine J, et al. Characterization of cell fate probabilities in single-cell data with Palantir. Nat Biotechnol 2019;37:451–60.
[24] Hu H, Miao YR, Jia LH, et al. AnimalTFDB 3.0: a comprehensive resource for annotation and prediction of animal transcription factors. Nucleic Acids Res 2019;47:D33–8.
[25] Lachmann A, Giorgi FM, Lopez G, et al. ARACNe-AP: gene network reverse engineering through adaptive partitioning inference of mutual information. Bioinformatics 2016;32:2233–3235.
[26] Lefebvre C, Rajbhandari P, Alvarez MJ, et al. A human B-cell interactome identifies MYB and FOXM1 as master regulators of proliferation in germinal centers. Mol Syst Biol 2010;6:377.
[27] Aibar S, González-Blas CB, Moerman T, et al. SCENIC: single-cell regulatory network inference and clustering. Nat Methods 2017;14:1083–6.
[28] Skinnider MA, Squair JW, Kathe C, et al. Cell type prioritization in single-cell data. Nat Biotechnol 2021;39:30–4.
[29] Li L, Dong J, Yan L, et al. Single-cell RNA-seq analysis maps development of human germline cells and gonadal niche interactions. Cell Stem Cell 2017;20:858–73.
[30] Lee HJ, Yoon JW, Jung KM, et al. Targeted gene insertion into Z chromosome of chicken primordial germ cells for avian sexing model development. FASEB J 2019;33:8519–29.
[31] Rengaraj D, Won S, Han JW, et al. Whole-transcriptome sequencing-based analysis of DAZL and its interacting genes during germ cells specification and zygotic genome activation in chickens. Int J Mol Sci 2020;21:8170.
[32] Rengaraj D, Won S, Jung KM, et al. Chicken blastoderms and primordial germ cells possess a higher expression of DNA repair genes and lower expression of apoptosis genes to preserve their genome stability. Sci Rep 2022;12:49.
[33] Zheng YH, Rengaraj D, Choi JW, et al. Expression pattern of meiosis associated SYCP family members during germline development in chickens. Reproduction 2009;138:483–92.
[34] Smith CA, Roeszler KN, Bowles J, et al. Onset of meiosis in the chicken embryo; evidence of a role for retinoic acid. BMC Dev Biol 2008;8:85.
[35] Guo C, Liu G, Zhao D, et al. Interaction of follicle-stimulating hormone and stem cell factor to promote primordial follicle assembly in the chicken. Front Endocrinol 2019;10:91.
[36] Richardson BE, Lehmann R. Mechanisms guiding primordial germ cell migration: strategies from different organisms. Nat Rev Mol Cell Biol 2010;11:37–49.
[37] Chawengsaksophak K, Svingen T, Ng ET, et al. Loss of wnt5a disrupts primordial germ cell migration and male sexual development in mice. Biol Reprod 2012;86:1–12.
[38] Clark AM, Garland KK, Russell LD. Desert hedgehog (Dhh) gene is required in the mouse testis for formation of adult-type Leydig cells and normal development of peritubular cells and seminiferous tubules. Biol Reprod 2000;63:1825–38.
[39] Wang X, Guo G, Zhang X, et al. Effect of RFRP-3, the mammalian ortholog of GnIH, on the epididymis of male rats. Theriogenology 2018;118:196–202.

[40] Li MW, Mruk DD, Cheng CY. Mitogen-activated protein kinases in male reproductive function. Trends Mol Med 2009;15:159–68.
[41] Whyte J, Glover JD, Woodcock M, et al. FGF, insulin, and SMAD signaling cooperate for avian primordial germ cell self-renewal. Stem Cell Rep 2015;5:1171–82.
[42] Lee HC, Lim S, Han JY. Wnt/β-catenin signaling pathway activation is required for proliferation of chicken primordial germ cells in vitro. Sci Rep 2016;6:34510.
[43] Jaroudi S, Kakourou G, Cawood S, et al. Expression profiling of DNA repair genes in human oocytes and blastocysts using microarrays. Hum Reprod 2009;24:2649–55.
[44] García-Rodríguez A, Gosálvez J, Agarwal A, et al. DNA damage and repair in human reproductive cells. Int J Mol Sci 2018;20:31.
[45] Kim SM, Yokoyama T, Ng D, et al. Retinoic acid-stimulated ERK1/2 pathway regulates meiotic initiation in cultured fetal germ cells. PLoS ONE 2019;14: e0224628.
[46] Endo T, Mikedis MM, Nicholls PK, et al. Retinoic acid and germ cell development in the ovary and testis. Biomolecules 2019;9:775.
[47] Nogueira D, Albano C, Adriaenssens T, et al. Human oocytes reversibly arrested in prophase I by phosphodiesterase type 3 inhibitor in vitro. Biol Reprod 2003;69:1042–52.
[48] Tosti E. Calcium ion currents mediating oocyte maturation events. Reprod Biol Endocrinol 2006;4:26.
[49] DiLuigi A, Weitzman VN, Pace MC, et al. Meiotic arrest in human oocytes is maintained by a Gs signaling pathway. Biol Reprod 2008;78:667–72.
[50] Johnson MT, Freeman EA, Gardner DK, et al. Oxidative metabolism of pyruvate is required for meiotic maturation of murine oocytes in vivo. Biol Reprod 2007;77:2–8.
[51] Knapczyk-Stwora K, Grzesiak M, Ciereszko RE, et al. The impact of sex steroid agonists and antagonists on folliculogenesis in the neonatal porcine ovary via cell proliferation and apoptosis. Theriogenology 2018;113:19–26.
[52] Pfeiffer J, Tarbashevich K, Bandemer J, et al. Rapid progression through the cell cycle ensures efficient migration of primordial germ cells - The role of Hsp90. Dev Biol 2018;436:84–93.
[53] Liu J, Wang QC, Han J, et al. Aflatoxin B1 is toxic to porcine oocyte maturation. Mutagenesis 2015;30:527–35.
[54] Xu W, Guo G, Li J, et al. Activation of Bcl-2-caspase-9 apoptosis pathway in the testis of asthmatic mice. PLoS ONE 2016;11:e0149353.
[55] Shen XH, Jin YX, Liang S, et al. Autophagy is required for proper meiosis of porcine oocytes maturing in vitro. Sci Rep 2018;8:12581.
[56] Mo HQ, Tian FJ, Li X, et al. ANXA7 regulates trophoblast proliferation and apoptosis in preeclampsia. Am J Reprod Immunol 2019;82:e13183.
[57] Kelkar A, Dobberstein B. Sec61beta, a subunit of the Sec61 protein translocation channel at the endoplasmic reticulum, is involved in the transport of Gurken to the plasma membrane. BMC Cell Biol 2009;10:11.
[58] Kent J, Wheatley SC, Andrews JE, et al. A male-specific role for SOX9 in vertebrate sex determination. Development 1996;122:2813–22.
[59] Stebler J, Spieler D, Slanchev K, et al. Primordial germ cell migration in the chick and mouse embryo: the role of the chemokine SDF-1/CXCL12. Dev Biol 2004;272:351–61.
[60] Tsang SM, Oliemuller E, Howard BA. Regulatory roles for SOX11 in development, stem cells and cancer. Semin Cancer Biol 2020;67:3–11.
[61] Jung HG, Hwang YS, Park YH, et al. Role of epigenetic regulation by the REST/CoREST/HDAC corepressor complex of moderate NANOG expression in chicken primordial germ cells. Stem Cells Dev 2018;27:1215–25.
[62] Popowski M, Templeton TD, Lee BK, et al. Bright/Arid3A acts as a barrier to somatic cell reprogramming through direct regulation of Oct4, Sox2, and Nanog. Stem Cell Rep 2014;2:26–35.
[63] Sun J, Ting MC, Ishii M, et al. Msx1 and Msx2 function together in the regulation of primordial germ cell migration in the mouse. Dev Biol 2016;417:11–24.
[64] Itman C, Loveland KL. SMAD expression in the testis: an insight into BMP regulation of spermatogenesis. Dev Dyn 2008;237:97–111.
[65] Chen D, Liu W, Lukianchikov A, et al. Germline competency of human embryonic stem cells depends on eomesodermin. Biol Reprod 2017;97:850–61.
[66] Le Bouffant R, Souquet B, Duval N, et al. Msx1 and Msx2 promote meiosis initiation. Development 2011;138:5393–402.
[67] Ueda A, Akagi T, Yokota T. GA-binding protein alpha is involved in the survival of mouse embryonic stem cells. Stem Cells 2017;35:2229–38.
[68] Jørgensen A, Nielsen JE, Blomberg Jensen M, et al. Analysis of meiosis regulators in human gonads: a sexually dimorphic spatio-temporal expression pattern suggests involvement of DMRT1 in meiotic entry. Mol Hum Reprod 2012;18:523–34.
[69] Lee HJ, Seo M, Choi HJ, et al. DMRT1 gene disruption alone induces incomplete gonad feminization in chicken. FASEB J 2021;35:e21876.
[70] Hamazaki N, Kyogoku H, Araki H, et al. Reconstitution of the oocyte transcriptional network with transcription factors. Nature 2021;589: 264–9.
[71] Maekawa M, Yamaguchi K, Nakamura T, et al. Direct reprogramming of somatic cells is promoted by maternal transcription factor Glis1. Nature 2011;474:225–9.
[72] Rengaraj D, Hwang YS, Lee HC, et al. Zygotic genome activation in the chicken: a comparative review. Cell Mol Life Sci 2020;77:1879–91.
[73] Naora H, Naora H. Differential expression patterns of beta-actin mRNA in cells undergoing apoptosis. Biochem Biophys Res Commun 1995;211:491–6.
[74] Show MD, Hill CM, Anway MD, et al. Phosphorylation of mitogen-activated protein kinase 8 (MAPK8) is associated with germ cell apoptosis and redistribution of the Bcl2-modifying factor (BMF). J Androl 2008;29:338–44.
[75] Bagheri-Yarmand R, Sinha KM, Gururaj AE, et al. A novel dual kinase function of the RET proto-oncogene negatively regulates activating transcription factor 4-mediated apoptosis. J Biol Chem 2015;290:11749–61.
[76] Slaughter GR, Meistrich ML, Means AR. Expression of RNAs for calmodulin, actins, and tubulins in rat testis cells. Biol Reprod 1989;40:395–405.
[77] Ray D, Hogarth CA, Evans EB, et al. Experimental validation of Ankrd17 and Anapc10, two novel meiotic genes predicted by computational models in mice. Biol Reprod 2012;86:102.
[78] Zhou L, Yang Y, Zhang J, et al. The role of RING box protein 1 in mouse oocyte meiotic maturation. PLoS ONE 2013;8:e68964.
[79] Lobascio AM, Klinger FG, Scaldaferri ML, et al. Analysis of programmed cell death in mouse fetal oocytes. Reproduction 2007;134:241–52.
[80] Ghafari F, Gutierrez CG, Hartshorne GM. Apoptosis in mouse fetal and neonatal oocytes during meiotic prophase one. BMC Dev Biol 2007;7:87.
[81] Pepling ME, Spradling AC. Mouse ovarian germ cell cysts undergo programmed breakdown to form primordial follicles. Dev Biol 2001;234:339–51.
[82] Yu N, Song Z, Zhang K, et al. MAD2B acts as a negative regulatory partner of TCF4 on proliferation in human dermal papilla cells. Sci Rep 2017;7:11687.
[83] Gaskell TL, Esnal A, Robinson LL, et al. Immunohistochemical profiling of germ cells within the human fetal testis: identification of three subpopulations. Biol Reprod 2004;71:2012–21.
[84] Le Bouffant R, Guerquin MJ, Duquenne C, et al. Meiosis initiation in the human ovary requires intrinsic retinoic acid synthesis. Hum Reprod 2010;25:2579–90.
[85] Eildermann K, Aeckerle N, Debowski K, et al. Developmental expression of the pluripotency factor sal-like protein 4 in the monkey, human and mouse testis: restriction to premeiotic germ cells. Cells Tissues Organs 2012;196:206–20.
[86] Dunne OM, Davies OR. Molecular structure of human synaptonemal complex protein SYCE1. Chromosoma 2019;128:223–36.
[87] Gill ME, Hu YC, Lin YF, et al. Licensing of gametogenesis, dependent on RNA binding protein DAZL, as a gateway to sexual differentiation of fetal germ cells. Proc Natl Acad Sci USA 2011;108:7443–8.
[88] Zuo Q, Li D, Zhang L, et al. Study on the regulatory mechanism of the lipid metabolism pathways during chicken male germ cell differentiation based on RNA-seq. PLoS ONE 2015;10:e0109469.
[89] Guo J, Grow EJ, Yi C, et al. Chromatin and single-cell rna-seq profiling reveal dynamic signaling and metabolic transitions during human spermatogonial stem cell development. Cell Stem Cell 2017;21:533–546.e6.
[90] Green CD, Ma Q, Manske GL, et al. A comprehensive roadmap of murine spermatogenesis defined by single-cell RNA-seq. Dev Cell 2018;46:651–67.
[91] Hermann BP, Cheng K, Singh A, et al. The mammalian spermatogenesis single-cell transcriptome, from spermatogonial stem cells to spermatids. Cell Rep 2018;25:1650–67.
[92] Wang M, Liu X, Chang G, et al. Single-cell RNA sequencing analysis reveals sequential cell fate transition during human spermatogenesis. Cell Stem Cell 2018;23:599–614.
[93] Zhang X, Li X, Li R, et al. Transcriptomic profile of early zebrafish PGCs by single cell sequencing. PLoS ONE 2019;14:e0220364.
[94] Lackner DH, Carré A, Guzzardo PM, et al. A generic strategy for CRISPR-Cas9-mediated gene tagging. Nat Commun 2015;6:10237.
[95] Suzuki K, Tsunekawa Y, Hernandez-Benitez R, et al. In vivo genome editing via CRISPR/Cas9 mediated homology-independent targeted integration. Nature 2016;540:144–9.
[96] West JA, Viswanathan SR, Yabuuchi A, et al. A role for Lin28 in primordial germ-cell development and germ-cell malignancy. Nature 2009;460:909–13.
[97] Zhao R, Zuo Q, Yuan X, et al. Production of viable chicken by allogeneic transplantation of primordial germ cells induced from somatic cells. Nat Commun 2021;12:2989.
[98] Naeemipour M, Dehghani H, Bassami M, et al. Expression dynamics of pluripotency genes in chicken primordial germ cells before and after colonization of the genital ridges. Mol Reprod Dev 2013;80:849–61.
[99] Raucci F, Fuet A, Pain B. In vitro generation and characterization of chicken long-term germ cells from different embryonic origins. Theriogenology 2015;84:732–42.
[100] Mayere C, Neirijnck Y, Sararols P, et al. Single-cell transcriptomics reveal temporal dynamics of critical regulators of germ cell fate during mouse sex determination. FASEB J 2021;35:e21452.